FACULTY OF INFORMATION TECHNOLOGY AND ELECTRICAL ENGINEERING

DEGREE PROGRAMME IN ELECTRONICS AND COMMUNICATIONS ENGINEERING

MASTER'S THESIS

ON FEASIBILITY OF THE UE POWER SAVING SIGNAL FOR THE 5G NEW RADIO

Author   Juho Lahdenperä

Supervisor   Pekka Pirinen

Second Examiner   Markku Juntti

Technical Advisor   Sami Hakola

May 2019

ABSTRACT

The objective of this thesis is to study and evaluate physical layer signals and channels to achieve the user equipment (UE) power saving in the 3rd generation partnership project (3GPP) new radio (NR). The fifth generation (5G) mobile network has strict objectives regarding power consumption and performance. The UE power consumption also has a big impact on the end user's quality of experience (QoE) and future deployment of NR devices. Therefore, it is very important to study ways to reduce UE power consumption. One feasible power saving technique is the usage of so-called power saving signal or channel, which triggers the UE to transition to the active mode from the power saving mode.

The first part of this work provides an overview of general properties of the NR and its physical downlink signals and channels, as well as the UE operation and power consumption in the connected mode. Then, examples of existing power saving techniques are discussed and a new scheme of the wake-up mechanism and the UE power saving signal/wake-up signal (WUS) is described. Lastly, different design options for the power saving signal are described and their detection performance is studied.

The power saving signal options of this thesis can be divided into physical downlink control channel (PDCCH) based and sequence-based signals/channels. In the PDCCH based option, the power saving indication is carried as a payload of the PDCCH. Studied sequence-based options are the secondary synchronization signal (SSS), the PDCCH demodulation reference signal (DMRS), the channel state information reference signal (CSI-RS) and a UE-specific sequence that is mapped to all radio resources allocated for the PDCCH. The detection of the latter is done in time domain, and the detection of the other sequences is done in frequency domain.

The detection performance of these signals/channels is compared based on link-level simulation results. Simulations were done with a Matlab-based simulator. They show the impact of the frequency- and time-selectivity and implementation impairments. Based on the numerical results, the impact of the UE speed up to 120 km/h and the carrier frequency offset (CFO) up to 400 Hz can be neglected with all the options except CSI-RS. It was shown that the sequence-based WUS options tend to suffer from the frequency-selective radio channel. By making decisions within the channel's coherence bandwidth and using precoder cycling, the negative impact of the channel can be reduced. With these techniques, PDCCH DMRS outperforms all the other sequence-based options. However, in terms of detection performance, the PDCCH based power saving signal/channel is the most robust option of this set of candidates.

Key words: wake-up signal, WUS.

TIIVISTELMÄ

Tämän diplomityön tavoitteena on tutkia ja verrata fyysisen kerroksen signaaleja, päätelaitteen (user equipment, UE) virransäästön toteuttamiseksi 3GPP:n uudessa radiorajapinnassa (New Radio, NR). Viidennen sukupolven (5th generation, 5G) mobiiliverkolla on tiukat tavoitteet virransäästön ja suorituskyvyn osalta. Päätelaitteen virrankulutuksella on myös suuri vaikutus loppukäyttäjän kokemukseen ja tulevien NR-laitteiden käyttöönottoon. Siksi onkin erittäin tärkeää tutkia mahdollisia tapoja vähentää päätelaitteen virrankulutusta. Yksi mahdollinen virransäästötekniikka on niin sanottu virransäästösignaali, joka herättää päätelaitteen virransäästötilasta verkkoyhteyteen.

Työn ensimmäinen osa käsittelee NR:n yleisiä ominaisuuksia, alalinkin fyysisiä signaaleja ja kanavia, sekä päätelaitteen virrankulutusta verkkoyhteydessä. Seuraavaksi käsitellään olemassa olevia virransäästötekniikoita, sekä käydään läpi uutta herätys-tyyppistä mekanismia ja päätelaitteen virransäästösignaalin/herätyssignaalin (wake-up signal, WUS) toimintaa. Lopuksi kuvataan erilaisia virransäästösignaalivaihtoehtoja ja tutkitaan niiden havaitsemisen suorituskykyä.

Työn virransäästösignaalivaihtoehdot voidaan jakaa alalinkin kontrollikanava-(physical downlink control channel, PDCCH) ja sekvenssipohjaisiin signaaleihin/kanaviin. PDCCH-pohjaisessa vaihtoehdossa virransäästösignaali siirretään PDCCH:n hyötykuormana. Tutkitut sekvenssipohjaiset vaihtoehdot ovat toissijainen synkronointisignaali (secondary synchronization signal, SSS), PDCCH-demodulaatio-referenssisignaali (demodulation reference signal, DMRS), kanavan tilatieto-referenssisignaali (channel-state information reference signal, CSI-RS), sekä UE-spesifinen sekvenssi, joka asetetaan PDCCH:n jokaiseen alikantoaaltoon. Jälkimmäisen havaitseminen tehdään aikatasossa ja muiden sekvenssien havaitseminen tehdään taajuustasossa.

Näiden signaalien/kanavien havaitsemisen suorituskykyä vertaillaan linkkitason simulointitulosten perusteella. Simulaatiot tehtiin Matlab-pohjaisella simulaattorilla. Ne esittävät aika- ja taajuusselektiivisyyden, sekä toteutuksen epäideaalisuuksien vaikutusta. Numeeristen tulosten perusteella, UE:n nopeus arvoon 120 km/h ja kantoaaltotaajuussiirto (carrier frequency offset, CFO) 400 Hz:iin asti voidaan jättää huomioimatta, kaikkien muiden paitsi CSI-RS:n tapauksessa. Työssä osoitettiin, että sekvenssipohjaiset WUS-vaihtoehdot kärsivät taajuusselektiivisestä radiokanavasta. Kanavan negatiivista vaikutusta voidaan pienentää tekemällä päätöksiä kanavan koherenssikaistanleveyttä pienemmissä osissa, sekä käyttämällä syklistä esikooderia. Näillä tekniikoilla PDCCH DMRS suoriutuu kaikkia muita sekvenssipohjaisia vaihtoehtoja paremmin. Kuitenkin, havaitsemisen suorituskyvyn perusteella PDCCH-pohjainen virransäästösignaali/kanava on vahvin ehdokas näistä vaihtoehdoista.

Avainsanat: herätyssignaali, WUS.

TABLE OF CONTENTS

FOREWORD

This Master's Thesis was done at Nokia Bell Labs, Radio Interface Group located in Oulu, Finland from December 2018 to May 2019. The objective of this work was to study the feasibility of the UE power saving signal for the 5G New Radio. The analysis is based on 3GPP NR compliant link-level simulations and this work was done as a part of the RAN1 standardization project.

At first, I want to thank my Manager Jari Hulkkonen for the great opportunity to work as a thesis worker in his team. I would also like to thank my technical advisor, Senior Specialist Sami Hakola, as well as Senior Specialist Juha Karjalainen for their technical guidance and insight during this process. In addition, I want to thank Senior Specialist Pasi Kinnunen for the technical assistance and the whole team for their support.

Furthermore, I would like to express my gratitude to the supervisor of this thesis, Adjunct Professor Pekka Pirinen for all the instructions and help. Also, I would like to thank the second examiner of this thesis, Professor Markku Juntti.

Oulu, May 9, 2019

Juho Lahdenperä

LIST OF SYMBOLS AND ABBREVIATIONS

3GPP	3rd generation partnership project
5G	5th generation
AL	aggregation level
AWGN	additive white Gaussian noise
BPSK	binary phase shift keying
BW	bandwidth
BWP	bandwidth part
CBW	carrier bandwidth
CCE	control channel element
CFO	carrier frequency offset
CN	core network
CORESET	control resource set
CP	cyclic prefix
CRC	cyclic redundancy check
CSI-RS	channel state information reference signal
DCI	downlink control information
DFT	discrete Fourier transform
DMRS	demodulation reference signal
DRX	discontinuous reception
eMBB	enhanced mobile broadband
FFT	fast Fourier transform
gNB	g Node B
GTS	go-to-sleep signal
ICI	inter-carrier interference
IEEE	institute of electrical and electronics engineers
IFFT	inverse fast Fourier transform
IoT	internet of things
ISI	inter-symbol interference
ITU-R	radiocommunication sector of international telecommunication union
LOS	line of sight
LTE	long-term evolution
MAC	medium access control
MIB	master information block
MIMO	multiple input multiple output
mMTC	massive machine-type communication
NLOS	non-line of sight
NR	new radio
OFDM	orthogonal frequency-division multiplexing
PBCH	physical broadcast channel
PCI	physical cell identity

PDCCH	physical downlink control channel
PDSCH	physical downlink shared channel
PMD	probability of miss-detection
PRB	physical resource block
PSS	primary synchronization signal
PTRS	phase tracking reference signal
QAM	quadrature amplitude modulation
QoE	quality of experience
QPSK	quadrature phase shift keying
RE	resource element
REG	resource-element group
RF	radio frequency
RMS	root mean square
RRC	radio resource control
RS	reference signal
RX	receiver
SCS	subcarrier spacing
SNR	signal-to-noise ratio
SRS	sounding reference signal
SSB	synchronization signal block
SSS	secondary synchronization signal
TDL	tapped delay line
TDM	time-division multiplexing
TRS	tracking reference signal
TX	transmitter
UE	user equipment
URLLC	ultra-reliable and low latency communication
VoIP	voice over internet protocol
WLAN	wireless local area network
WUS	wake-up signal

B_D	Doppler spread of the channel
$c(n)$	pseudo random sequence
c_init	initialization value
$c_\mathrm{init}^\mathrm{CSI\text{-}RS}$	CSI-RS initialization value
$c_\mathrm{init}^\mathrm{PBCH}$	PBCH DMRS initialization value
$c_\mathrm{init}^\mathrm{PDCCH}$	PDCCH DMRS initialization value
$c_\mathrm{init}^\mathrm{PDSCH}$	PDSCH DMRS initialization value
$d_\mathrm{PSS}(n)$	PSS sequence
$d_\mathrm{SSS}(n)$	SSS sequence
f_D	maximum Doppler shift
l	OFDM symbol number within a slot

L	maximum number of SSB beams in an SSB period
$N_{\mathrm{ID}}^{(\mathrm{cell})}$	physical-layer cell identity
N_{PRB}	number of PRBs
$N_{\mathrm{symb}}^{\mathrm{slot}}$	number of symbols per slot
n_{hf}	number of the half-frame
$n_{\mathrm{s,f}}^{\mu}$	number of slots within a frame
$r(m)$	generic QPSK sequence
T_{m}	multipath spread of the channel
$\bar{v}$	velocity
λ_0	wavelength
Δf	subcarrier spacing
$(\Delta f)_c$	coherence bandwidth of the channel
$(\Delta t)_c$	coherence time of the channel
μ	subcarrier spacing configuration

1   INTRODUCTION

The first generation of mobile communication emerged around 1980. Since then, the world has seen a new generation of mobile communication roughly in every ten years. The second generation, emerging in the early 1990's, introduced digital transmission on the radio link, with limited data services. The third generation of mobile communication, introduced in early 2000, was the first to enable a fast wireless internet access due to the high-quality mobile broadband. In the fourth generation, represented by the long-term evolution (LTE) technology, the mobile-broadband experience is then further enhanced in terms of higher achievable data rates. In 2009, the first release of the LTE technical specifications was released, and already around 2012, discussions on the fifth generation (5G) mobile communication began. [1]

The term 5G is often used to refer to the specific new radio-access technology, but it is also used in a much wider context referring to many new services envisioned to be enabled by the 5G. To categorize the capabilities of the 5G-network, the radiocommunication sector of the international telecommunication union (ITU-R) has divided usage scenarios into three categories. The usage scenarios are enhanced mobile broadband (eMBB), ultra-reliable and low latency communication (URLLC) and massive machine-type communication (mMTC). The usage scenario of eMBB covers a wide range of cases from hotspots with high traffic capacity and data-rates to the improved wide-area coverage. URLLC usage scenarios include cases like remote medical surgery and wireless control over industrial factories. Because of the critical nature of URLLC cases, they tend to have very strict requirements regarding throughput, availability and latency. Lastly, mMTC is a usage scenario, intended to support a massive amount of internet of things (IoT) devices with low cost, long battery life and non-delay-sensitive data. [2]

Although LTE is a very capable network, it cannot support the whole new set of usage scenarios, with performance requirements like lower latency, better reliability, massive connectivity and higher energy efficiency [3]. To answer the set of new requirements, the third generation partnership project (3GPP) has introduced a 5G-network with a new air interface, called the new radio (NR) [1][3].

Because the UE battery life has a big impact on the user's quality of experience (QoE) and the future adaptation of 5G NR devices and services, it is important to research techniques to decrease UE power consumption. When comparing power consumption of the mobile communication generations, the trend has been that energy efficiency has generally improved [4]. This trend is designed to continue in 5G NR, since ITU-R states in the recommendation M.2083-0 [2] that the next generation radio access network should deliver enhanced capabilities, while energy consumption should not be greater than in current networks. [5]

The objective of this work is to study and evaluate the physical layer signals to facilitate UE power saving in 3GPP New Radio. Because the NR system may be capable of supporting high speed data transport, it is expected that the user data tends to be bursty and served in very short durations [5]. One efficient UE power saving mechanism is to trigger the UE for network access from a power efficient mode using the new power saving signal [5]. The UE would stay in the power efficient mode, unless it is informed of network access through the UE power saving signal. In this thesis, different options of physical signals and channels for the power saving signal usage are analyzed from the perspective of the UE and the network. The analysis is based on 3GPP NR compliant link-level simulations and evaluation metrics include miss detection probability, false alarm rate as well as the impact on latency and the network.

This thesis is organized as follows. Chapter 2 reviews the basics of the 5G NR, its physical layer and operation in the RRC_CONNECTED mode. Chapter 3 deals with different power

saving techniques and explains the principle and design of the wake-up signal. Chapter 4 presents the simulation cases and parameters, as well as operating principles of the used simulator. In Chapter 5, numerical results of the wake-up signal simulations are presented. Simulation results and observations are further discussed in Chapter 6. Finally, Chapter 7 summarizes the thesis.

2   PHYSICAL LAYER OF 5G NEW RADIO

Physical layer is the first layer of the NR radio interface protocol architecture. Physical layer provides data transport services to higher layers. Transport services are accessed through transport channels between the physical layer and the medium access control (MAC) part of layer two. The data transport service of the physical layer includes for example coding, modulation/demodulation, multi-antenna processing and mapping of the coded transport channel to the correct physical channels. In addition to the layer two, the physical layer also interfaces with the radio resource control (RRC) part of the layer three. [6]

The first part of this chapter reviews the general properties of the NR physical layer. The second part provides an overview of the physical downlink channels and signals provided by the physical layer. The last part of this chapter deals with the UE's power consumption and operation in the RRC_CONNECTED mode.

2.1   General Properties

The NR uses orthogonal frequency-division multiplexing (OFDM) as a waveform in both the uplink and the downlink transmission directions [1]. OFDM provides a flexible multiple-access scheme, where the available bandwidth (BW) is divided into mutually orthogonal subcarriers, which can be shared amongst multiple users without intra-cell interference [7]. OFDM is nowadays a broadly adopted technology that is suitable also for the NR because of the merits like low complexity, plain channel estimation and easy multiple-input and multiple-output (MIMO) -integration [8]. In addition, the uplink transmission scheme has also a possibility to use discrete Fourier transform (DFT) -precoded OFDM as a waveform [1]. DFT-precoded OFDM is used to obtain higher power-amplifier efficiency. However, DFT-precoded OFDM is used only as a complementary support, because of the several drawbacks. DFT-precoding increases the complexity of MIMO-receivers and restricts scheduling in the frequency domain. [1]

With only one OFDM numerology, the NR could not fulfil the performance requirements of the wide range of applications, devices and carrier frequencies [9]. For this reason, the NR supports multiple OFDM numerologies with a range of subcarrier spacings (SCSs). The supported subcarrier spacings are 15, 30, 60, 120 and 240 kHz, but 240 kHz is only supported by the synchronization signal block (SSB), which is further described in Section 2.2.2. The flexible numerology is based on scaling, where subcarrier spacing of 15 kHz is the baseline. [1] The baseline of 15 kHz was chosen, so that the NR supports efficient coexistence with LTE [1]. Scaling of the subcarrier spacing from the baseline is defined as

$$\Delta f = 2^{\mu} \times 15 \text{ kHz,} \tag{1}$$

where the subcarrier spacing configuration μ is an integer between 0-4 and comes from the higher-layer parameter *subcarrierSpacing* [10]. Subcarrier spacings with proportional symbol and cyclic prefix (CP) durations are presented in Table 1. Therein, symbol and cyclic prefix durations depend on the subcarrier spacing. The duration of the symbol and cyclic prefix scales from the baseline by powers of two. [1]

Table 1. Supported subcarrier spacings with proportional symbol and CP durations.

Subcarrier spacing configuration (μ)	Δf [kHz]	Symbol duration [μs]	Cyclic prefix duration [μs]
0	15	66.7	4.7
1	30	33.3	2.3
2	60	16.7	1.2
3	120	8.33	0.59
4	240	4.17	0.29

The frame structure of the NR is as follows. NR transmissions are organized into 10 ms long frames. Each frame is then divided into ten subframes and they are further divided into slots. Each slot consists of 14 OFDM symbols in the time domain and 12 subcarriers in the frequency domain. An exception to this is the 60 kHz subcarrier spacing with an extended CP, where each slot consists of 12 OFDM symbols and 12 subcarriers. The extended CP for 60 kHz can be used when it is needed to reduce the slot duration and delay while maintaining a CP similar to 15 kHz. In the time domain, the slot length in milliseconds is defined as

$$\text{Slot length} = 1 \text{ ms}/2^{\mu}, \tag{2}$$

where μ is the subcarrier spacing configuration. Based on (2), the slot's bandwidth in frequency domain and the length in time domain scale with the baseline by powers of two. The number and the length of slots with the supported SCSs is presented in Table 2. When the subcarrier spacing is doubled, the number of slots within a subframe is also doubled. [1][10][11]

Table 2. Number and length of slots with the supported subcarrier spacings.

Subcarrier spacing configuration (μ)	Number of symbols in a slot	Number of slots in a subframe	Number of slots in a frame	Slot length [ms]
0	14	1	10	1
1	14	2	20	0.5
2	14 (normal CP) 12 (extended CP)	4	40	0.25
3	14	8	80	0.125
4	14	16	160	0.0625

The time-division multiplexing (TDM) scheme in the NR is more flexible than for example TDM in LTE [8]. OFDM symbols in a slot are classified as 'uplink', 'downlink' or 'flexible' [10]. The 'flexible' slot is a combination of uplink and downlink symbols [8] [10]. The UE assumes that the downlink transmission occurs only in 'downlink' or 'flexible' symbols and thus it transmits only in 'uplink' or 'flexible' symbols [10].

In addition to the three configured slot types, the NR supports so-called mini-slots. Mini-slots can be used to support shorter transmissions, since a mini-slot can be as short as one OFDM symbol in time. A mini-slot can also start at any time within a slot to enable a more flexible start position in the time domain. In order to obtain low latency, the beginning of the slot can also be front-loaded with control and reference signals (RSs). Because of the flexible time structure of the mini-slots, they can be used for example in low-latency scenarios, where the transmission needs to start immediately. [12]

In the frequency domain, physical resource blocks (PRBs) are the basic scheduling units of the NR [8]. One PRB is composed of 12 subcarriers, which have the same subcarrier spacing

and CP overhead within a PRB. Each individual element, grouped into one subcarrier of the PRB, is called a resource element (RE) [10]. The RE is the smallest unit in the resource grid. It corresponds to a physical resource made up of one OFDM symbol in time and one subcarrier in frequency. So, a PRB is composed of 12 REs and they are uniquely identified in the frequency/time domain of the PRB [10].

An example of the NR frame structure with the subcarrier spacings of 15, 30 & 60 kHz is presented in Figure 1. It illustrates how doubling the SCS doubles the bandwidth and halves the slot duration. As can be seen, with a higher SCS, more slots fit into one subframe.

1 Frame = 10 Subframes

1 Slot = 14 OFDM Symbols x 12 Subcarriers

1 Subframe = 1/2/4/8/16 Slots

1 RE

Frame (10 ms)

Subframe (1 ms)

SLOT (1 ms)

$\mu = 0$
$(12 \times 15 \text{ kHz})$

SLOT (0.5 ms)

$\mu = 1$
$(12 \times 30 \text{ kHz})$

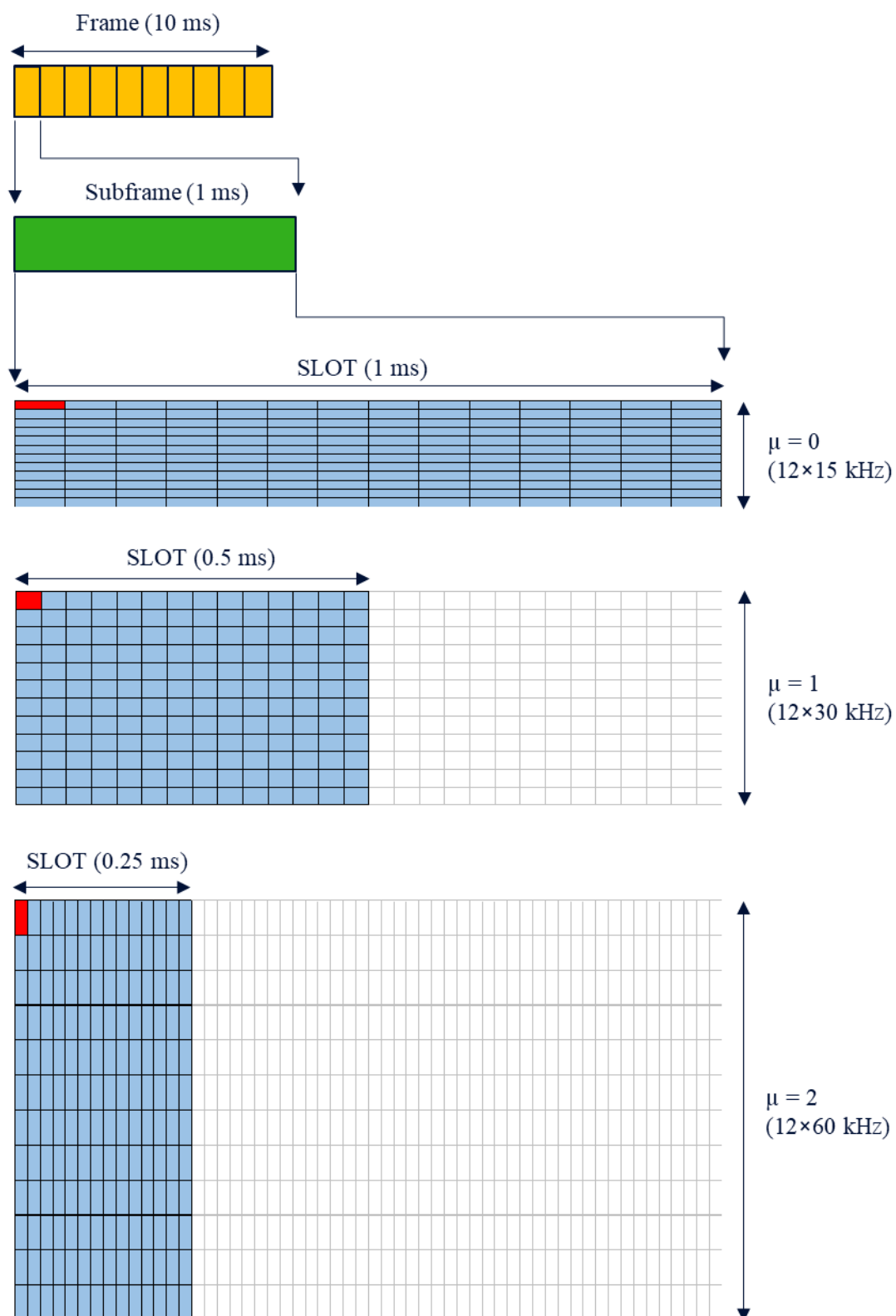SLOT (0.25 ms)

$\mu = 2$
$(12 \times 60 \text{ kHz})$

Figure 1. 5G NR frame structure.

2.2 Overview of Physical Downlink Channels and Signals

The physical layer of the NR has multiple downlink physical channels and signals for information, control and data transmission purposes. The physical downlink channel corresponds to a set of REs carrying information that originates from higher layers [10]. The physical downlink signal corresponds to a set of REs carrying information, which does not originate from higher layers [10]. This section provides an overview to these channels and signals.

2.2.1 Reference Signals

Reference signals are predefined downlink signals, which are used for different purposes [1]. The design of the NR reference signals is based on flexible time/frequency allocation and an on-demand principle [13]. Flexibility and the on-demand principle provide forward compatibility and reduce energy consumption and intercell interference [13]. The NR has several types of reference signals: the demodulation reference signal (DMRS), the phase-tracking reference signal (PTRS), the channel-state information reference signal (CSI-RS), the tracking reference signal (TRS) and the sounding reference signal (SRS) [1]. The purpose of the DMRS and PTRS signals is introduced below, while the CSI-RS, TRS and SRS signals are described in Section 2.2.5.

DMRS is a physical signal that provides channel estimates of the associated physical channel. Each physical channel has a specific design of DMRS and it is used by the receiver (RX) for the demodulation of the corresponding channel. DMRS is always UE specific and transmitted on demand. [13]

The purpose of the PTRS is to provide a means to compensate the oscillator phase noise. In an OFDM signal, phase noise usually causes identical phase rotation to all the subcarriers, so it is beneficial to provide a UE-specific reference to compensate it. In many cases, phase noise increases as a function of the carrier frequency. PTRS can be configured differently, depending on the quality of the used oscillators, SCS, carrier frequency, modulation and coding. [12]

The NR uses pseudo-random sequences in many of the reference signals [10]. Based on use-case of the RS, the generation of the pseudo-random sequence is initialized differently. Generic pseudo-random sequences in the NR are defined by a 31 element long Gold sequence. The generation of the pseudo-random sequence $c(n)$ of the length M is defined as

$$c(n) = \left(x_1(n + N_c) + x_2(n + N_c)\right)\mathrm{mod}\,2, \tag{3}$$

where

$$x_1(n + 31) = \left(x_1(n + 3) + x_1(n)\right)\mathrm{mod}\,2 \tag{4}$$

and

$$x_2(n + 31) = \left(x_2(n + 3) + x_2(n + 2) + x_2(n + 1) + x_2(n)\right)\mathrm{mod}\,2 \tag{5}$$

in which $n = 0, 1, \ldots, M - 1$, $N_c = 1600$ and $x_1(n)$ is initialized as follows: $x_1(0) = 1$, $x_1(n) = 0$. Finally, $x_2(n)$ is initialized with the initialization value

$$c_{\text{init}} = \sum_{i=0}^{30} x_2(i) \times 2^i, \tag{6}$$

where the initialization value c_{init} depends on the application of the sequence $c(n)$. [10]

The modulation of the multiple NR's reference signals is quadrature phase shift keying (QPSK). The generation of a generic QPSK sequence $r(m)$ is defined as

$$r(m) = \frac{1}{\sqrt{2}}\left(1 - 2 \times c(2m)\right) + j\frac{1}{\sqrt{2}}\left(1 - 2 \times c(2m+1)\right), \tag{7}$$

where $c(n)$ is the pseudo-random sequence defined in (3). [10]

2.2.2 Synchronization Signal Block

Cell search is a part of the initial-access functionalities of the NR [1]. Cell search covers the procedures for a UE to find new cells [1]. The procedures include functions like acquiring time and frequency synchronization with a cell and detecting the physical layer cell ID of the cell [14]. Cell search is firstly carried out when a UE is initially entering to the system's coverage area [1]. Secondly, cell search is continuously carried out by moving UEs within the system's coverage [1]. In order to perform cell search, the UE receives periodically two synchronization signals, the primary synchronization signal (PSS) and the secondary synchronization signal (SSS) [1], [14]. PSS and SSS, together with the physical broadcast channel (PBCH), form a synchronization signal block (SSB) [1][14]. Additionally, SSB has the DMRS for the PBCH mapped to each fourth subcarrier of the PBCH symbols [10].

The time/frequency structure of the SSB, consisting of PSS, SSS and PBCH, is illustrated in Figure 2. An SSB consists of 240 subcarriers (20 PRBs) in the frequency domain, numbered from 0 to 239. In the time domain, an SSB consists of four OFDM symbols, numbered from 0 to 3. The center frequency of the PSS and SSS is the same as the center frequency of the PBCH [15]. PSS is transmitted in the first OFDM symbol. PSS occupies 127 subcarriers and the remaining subcarriers in the sides are empty. SSS is transmitted in the third OFDM symbol and it also occupies 127 subcarriers. Sides of the SSS have eight and nine empty subcarriers. PBCH is transmitted in the second, fourth and partially in the third OFDM symbol. PBCH occupies 240 subcarriers (20 PRBs) in the second and fourth symbol, and 48 subcarriers on each side of the SSS. [1], [10]
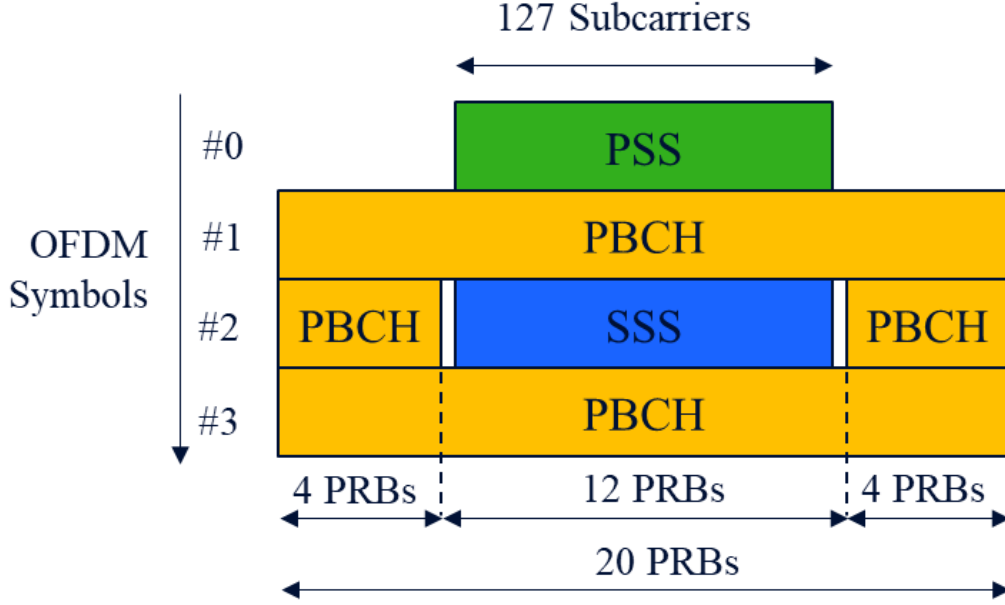
Figure 2. The time/frequency structure of the SSB.

PSS is the first signal that a UE searches, when entering to the NR system [1]. PSS is designed so that its detection is possible despite uncertainties in the system, such as deviations between devices and the network's carrier frequency [1]. After detecting PSS, the UE can synchronize its internal frequency generation based on transmissions from the network, as well as reduce frequency deviation between them [1]. The PSS sequence $d_{\text{PSS}}(n)$ is based on an m-sequence and it is defined as

$$d_{\text{PSS}}(n) = 1 - 2x(m), \tag{8}$$

where $0 \leq n < 127$, and symbols x and m are defined as

$$x(i + 7) = (x(i + 4) + x(i))\text{mod}2, \tag{9}$$

$$[x(6)\, x(5)\, x(4)\, x(3)\, x(2)\, x(1)\, x(0)] = [1\ 1\ 1\ 0\ 1\ 1\ 0] \tag{10}$$

and

$$m = (n + 43N_{\text{ID}}^{(2)})\text{mod}127 \tag{11}$$

where $N_{\text{ID}}^{(2)}$ comes from the physical cell identity (PCI) of the cell [10].

PCI determines which PSS and SSS sequences the cell uses. There are totally three different PSS sequences and 336 different SSS sequences, so that the total number of unique PCIs is 1008 [1]. Physical-layer cell identities $N_{\text{ID}}^{(\text{cell})}$ are given by

$$N_{\text{ID}}^{(\text{cell})} = 3N_{\text{ID}}^{(1)} + N_{\text{ID}}^{(2)} \tag{12}$$

where $N_{\text{ID}}^{(1)} \in \{0, 1, \ldots, 335\}$ and $N_{\text{ID}}^{(2)} \in \{0, 1, 2\}$ [10].

After detecting PSS, the UE knows transmission timing of the SSS and is able to receive it. With already detected PSS and then detected SSS, the UE can determine the full PCI of the detected cell. The SSS sequence $d_{sss}(n)$ is composed of two m-sequences and it is defined as

$$d_{sss}(n) = [1 - x_0((n + m_0)\text{mod}127)][1 - 2x_1((n + m_1)\text{mod}127)], \qquad (13)$$

where two m-sequences m_0 and m_1 are defined as

$$m_0 = 15\left\lfloor\frac{N_{ID}^{(1)}}{112}\right\rfloor + N_{ID}^{(2)} \qquad (14)$$

and

$$m_1 = N_{ID}^{(1)}\text{mod}112, \qquad (15)$$

in which $0 \leq n < 127$ [10]. $N_{ID}^{(1)}$ and $N_{ID}^{(2)}$ come from the PCI defined in (12). Symbols x_0 and x_1 are initialized by

$$x_0(i + 7) = (x_0(i + 4) + x_0(i))\text{mod}2 \qquad (16)$$

and

$$x_1(i + 7) = (x_1(i + 1) + x_1(i))\text{mod}2, \qquad (17)$$

where

$$[x_0(6)\ x_0(5)\ x_0(4)\ x_0(3)\ x_0(2)\ x_0(1)\ x_0(0)] = [0\ 0\ 0\ 0\ 0\ 0\ 1] \qquad (18)$$

and

$$[x_1(6)\ x_1(5)\ x_1(4)\ x_1(3)\ x_1(2)\ x_1(1)\ x_1(0)] = [0\ 0\ 0\ 0\ 0\ 0\ 1]. \qquad (19)$$

The total lengths of the PSS and SSS sequences are 127. As illustrated in Figure 2 (page 17), the basic structure of the PSS and SSS is the same. In both cases, length-127 sequences are mapped into 127 contiguous subcarriers/REs of the corresponding OFDM symbol. [10]

The last part of the SSB is the PBCH. PBCH is a physical channel that carries the master information block (MIB) [1]. MIB contains information that the UE needs for acquiring the network's remaining system information broadcasts [1]. The total payload of the PBCH is 56 bits, including a 24-bit cyclic redundancy check (CRC) [15]. PBCH uses polar codes in channel coding and the coded MIB bits are mapped across the resource elements in the PBCH [15].

As discussed before, PBCH symbols have a DMRS mapped in each fourth subcarrier. The DMRS sequence $r(m)$ for SSB is defined by (7) in Section 2.2.1, where the generic pseudo-random sequence $c(i)$ is defined by (3). The sequence generator $c(n)$ is initialized at the beginning of each SSB occasion with the PBCH DMRS initialization value

$$c_{\text{init}}^{\text{PBCH}} = 2^{11}(\bar{i}_{\text{SSB}} + 1)\left(\left\lfloor \frac{N_{\text{ID}}^{(1)}}{4} \right\rfloor + 1\right) + 2^6(\bar{i}_{\text{SSB}} + 1) + (N_{\text{ID}}^{(2)} \bmod 4), \tag{20}$$

where $\bar{i}_{\text{SSB}} = i_{\text{SSB}} + 4n_{\text{hf}}$ for $L = 4$ and $\bar{i}_{\text{SSB}} = i_{\text{SSB}}$ for $L = 8$ or $L = 64$, and L is the maximum number of SSB beams in an SSB period and n_{hf} is the number of the half-frame in which PBCH is transmitted (0 = first half-frame, 1 = second half-frame). If $L = 4$, i_{SSB} is the two least significant bits of the SSB index. If $L = 8$ or 64, i_{SSB} is the three least significant bits of the SSB index. [10]

The maximum number of SSB beams in the SSB period L depends on the frequency range. For frequencies ≤ 3 GHz, $L = 4$, for the frequency range 3 GHz $\leq$ frequency ≤ 6 GHz, $L = 8$ and for the frequency range 6 GHz $\leq$ frequency ≤ 52.6 GHz, $L = 64$. As mentioned in Section 2.1, SSB supports even the 240 kHz SCS. With a larger SCS, the SSB beam sweeping can be performed faster, because of the shorter symbol duration. This can be used to improve coverage, because more beams can be swept within a given time. [16]

As mentioned in Section 2.1, SSB can be used for a rough estimation of path loss and channel quality. However, SSB has a limited bandwidth and a low duty cycle, so more complicated channel characteristics are provided in other signals. [1] A more detailed description of those signals is given in Section 2.2.5.

2.2.3 Physical Downlink Control Channel

The physical downlink control channel (PDCCH) is used to perform physical layer control functions. They include for example downlink broadcast scheduling, uplink/downlink unicast data transmission and signaling of various aperiodic and periodic transmission/reception triggers. [17]

The modulation of the PDCCH is QPSK and the channel coding is based on polar codes. PDCCH carries the downlink control information (DCI) as a part of its payload. DCI provides the necessary information for the UE to properly receive and decode downlink data transmission. DCI carries for example parameters that contain information about data scheduling, radio resource allocation, link adaptation and MIMO operation [18]. In addition to DCI, a 24-bit CRC is attached to the payload. The UE uses CRC to detect transmission errors and as an assistance at the decoder. [1]

In the frequency domain, PDCCH can be mapped continuously or non-continuously [20]. PDCCH consists of 1, 2, 4, 8 or 16 control channel elements (CCEs), which corresponds to the aggregation levels (ALs) 1, 2, 4, 8 and 16 [10][17]. One control channel element consists of six resource-element groups (REGs) [17]. One REG consists of 12 resource elements in frequency domain, so one REG equals one resource block [17]. Mapping of the CCE-to-REG can be either interleaved or non-interleaved, for frequency-diverse or frequency-selective transmission scenarios [1].

Downlink control signaling in the NR is based on control resource sets (CORESETs). The CORESET corresponds to a set of frequency/time resources, which can occur anywhere in a slot and frequency range of the carrier. Within the CORESET, the UE is supposed to decode candidate control channels, using one or more search spaces. Only one CCE-to-REG mapping can be configured for one CORESET, but it is possible for a network to configure multiple CORESETs with different mappings. This way, CORESETs can be configured based on prevailing conditions, whether they are frequency-diverse or frequency-selective. [1]

DMRS of the PDCCH is mapped to every fourth subcarrier in REG. The PDCCH DMRS sequence is generated in the same manner as PBCH DMRS in Section 2.2.2, but with the PDCCH DMRS initialization value

$$c_{\text{init}}^{\text{PDCCH}} = \left(2^{17}(N_{\text{symb}}^{\text{slot}} \times n_{\text{s,f}}^{\mu} + l + 1)(N_{\text{ID}} + 1) + 2N_{\text{ID}}\right)\text{mod}2^{31}, \tag{21}$$

where, $N_{\text{ID}} \in \{0, 1, \ldots, 65535\}$ and is given by the higher-layer parameter *pdcch-DMRS-scramblingID* if provided, and otherwise $N_{\text{ID}} = N_{\text{ID}}^{\text{cell}}$. $N_{\text{symb}}^{\text{slot}}$ is the number of symbols per slot, l is the OFDM symbol number within the slot and $n_{\text{s,f}}^{\mu}$ is the slot number within a frame. [10]

To achieve further diversity in control signaling, NR-PDCCH has adopted a precoder cycling diversity scheme [17]. Precoder cycling improves channel estimation performance of the PDCCH [17]. It is a technique that virtualizes multiple beams into one PDCCH antenna port. [19]. In precoder cycling, the precoder changes cyclically between REG bundles per CCE [15],[17]. Precoder granularity defines the number of REGs with the same DMRS precoder [14]. Granularity is provided by a higher layer parameter *precoderGranularity* [14].

2.2.4 *Physical Downlink Shared Channel*

After detecting a PDCCH with the configured DCI format, the UE can decode physical downlink shared channel (PDSCH) transmission based on the indicated DCI [21]. DCI determines for example transport block sizes, modulation order and target code rate for the PDSCH transmission [21]. PDSCH is the main physical channel for downlink data transmission [1]. In addition to the user data, PDSCH can transmit paging information, random-access response messages and parts of the system information [1].

PDSCH supports QPSK and quadrature amplitude modulation (QAM). Constellation sizes of the supported QAMs are 16QAM, 64QAM and 256QAM. Modulated symbols are mapped across subcarriers and OFDM symbols. PDSCH is rate-matched around transmitted SSBs and CORESETs of the PDCCH. PDSCH DMRS symbols are front-loaded and their location can be slot or non-slot based. In addition, extra DMRS symbols can be configured if needed. [15]

The PDSCH sequence is generated in the same manner as DMRSs of the PBCH and PDCCH in Sections 2.2.2-3, but the sequence generation is initialized with the PDSCH DMRS initialization value

$$c_{\text{init}}^{\text{PDSCH}} = \left(2^{17}(N_{\text{symb}}^{\text{slot}} \times n_{\text{s,f}}^{\mu} + l + 1)(2N_{\text{ID}}^{n_{\text{SCID}}} + 1) + 2N_{\text{ID}}^{n_{\text{SCID}}} + n_{\text{SCID}}\right)\text{mod}2^{31}, \tag{22}$$

where $N_{\text{symb}}^{\text{slot}}$ is the number of symbols per slot. Parameters $n_{\text{SCID}} \in \{0, 1\}$ and $N_{\text{ID}} \in \{0, 1, \ldots, 65535\}$ are given by the higher-layer parameters if provided, otherwise $n_{\text{SCID}} = 0$ and $N_{\text{ID}} = N_{\text{ID}}^{\text{(cell)}}$. Parameter l is the OFDM symbol number within a slot and $n_{\text{s,f}}^{\mu}$ is the slot number within a frame. [10]

PDSCH DMRS has two configurations for the physical resource mapping, type A and B, given by the higher-layer parameter *dmrs-Type* [10]. Type A is a slot-based mapping type, where DMRS is mapped to the fixed OFDM symbol, regardless of the PDSCH assignment [15]. Type B is a non-slot-based mapping type, where DMRS is mapped to the first OFDM symbol of the PDSCH [15]. In addition, the NR supports the configuration of additional DMRS symbols, in the case of for example high-speed scenarios [15].

Although not fully supported in Release 15, the NR is prepared to support distributed MIMO. With a distributed MIMO, the UE could receive multiple PDSCHs per slot, independently from multiple sources. PDSCHs could be divided between multiple sites, from which they are transmitted to the UE. Basically, distributed MIMO would enable simultaneous data transmission to one UE, from multiple transmission points. [1]

2.2.5   Channel State Information – Reference Signal

Channel sounding is a technique where the receiver measures or estimates radio channel characteristics from specific signals. The interesting characteristic can be for example the channel's impact to the transmitted signal in frequency, time and/or spatial domain, as well as path loss. Channel sounding in the NR is based on sounding reference signals (SRS) for the uplink and channel-state information reference signals (CSI-RS) for the downlink. [1]

The tracking reference signal (TRS) is one unique type of a resource set, which consists of multiple periodical non-zero-power-CSI-RSs. TRS is used to assist the UE to successfully receive downlink transmission. The use cases include fine time and frequency tracking, as well as path delay and Doppler spread tracking [15]. TRS also helps the UE to track and compensate variations in time and frequency domains, caused by the oscillator imperfections. [1]

The time/frequency structure of the CSI-RS/TRS is illustrated in Figure 3. The CSI-RS/TRS structure has always four symbols between symbols that carry CSI-RS/TRS, within a slot. However, the exact number of PRBs and OFDM symbols for the CSI-RS/TRS may vary. CSI-RS/TRS is mapped to each fourth subcarrier of the PRB carrying it, so the total density of CSI-RS/TRS is 1/4 per PRB. However, the mapping of the CSI-RS/TRS does not necessarily begin from the first symbol within a slot. Therefore, the numbering of the OFDM symbols in Figure 3 starts from N, where N presents a configured symbol within a slot. [1]
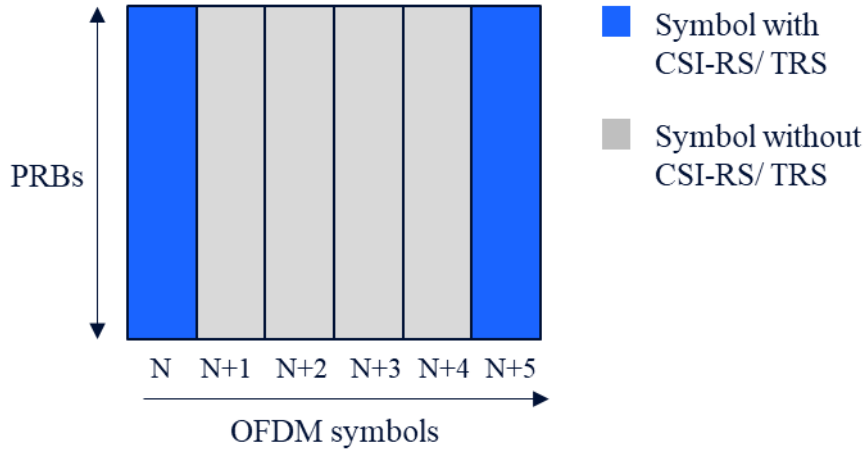

Figure 3. The time/frequency structure of the CSI-RS/TRS.

The CSI-RS/TRS sequence is generated in the same manner as DMRSs of the PBCH, PDCCH and PDSCH in Sections 2.2.2-4, but with the CSI-RS initialization value

$$c_{\text{init}}^{\text{CSI-RS}} = (2^{10}(N_{\text{symb}}^{\text{slot}} \times n_{\text{s,f}}^{\mu} + l + 1)(n_{\text{ID}} + 1) + 2n_{\text{ID}})\bmod 2^{31} \tag{23}$$

where n_{ID} is given by the higher-layer parameter *scramblingID* or *sequenceGenerationConfig*, l is the OFDM symbol number within a slot and $n_{s,f}^{\mu}$ is the slot number within a frame. The sequence generator c is initialized at the beginning of every OFDM symbol with $c_{init}^{CSI\text{-}RS}$. [10]

2.3   UE Operation and Power Consumption in CONNECTED Mode

In the NR system, the UE can be in three different radio resource control (RRC) states, RRC_IDLE, RRC_INACTIVE and RRC_CONNECTED. RRC_IDLE is a state where the device reduces power consumption by sleeping most of the time. No data transfer happens in this state, the device does not belong to a specific cell and uplink synchronization is not maintained. The RRC context is a set of parameters, which includes the necessary information for communication between the device and the network. In the RRC_IDLE state, there is no RRC context in the radio-access network. The RRC context is established when the device moves to a connected state. Random access is the only uplink transmission that the UE can use to move to a connected state. [1]

RRC_CONNECTED is a state intended for the uplink/downlink data transmission. In this state, the RRC context and all necessary parameters are known by the device and the radio-access network. The UE belongs to a known cell, identity of the device is configured, and mobility is handled by the radio-access network. When the UE is in a connected state, its power consumption can be reduced with discontinuous reception (DRX). DRX functionality reduces power consumption by turning off the radio frequency (RF) module, when there is no data transmission for the UE [24]. DRX and its operation is described in more detail in Section 3.1. [1]

Since LTE only supports connected and idle states, the idle state is used as a primary sleep state to reduce power consumption of the devices. However, due to the nature of modern smartphone data traffic, a significant amount of idle-to-active transitions happens in the core network. These transitions cause extra signaling load and delay to the network. To reduce these unnecessary transitions, the NR has also the third RRC state, RRC_INACTIVE. In the inactive state, the UE can sleep in a similar manner as in the idle state, but the RRC context and the core network connection are kept. This means that a transition from inactive to connected can be handled much faster than the transition from idle to connected. [1]

A state diagram of the NR's RRC states is presented in Figure 4. As illustrated, the device can switch fast between connected and inactive states, because the RRC context and the core network (CN) connection are kept in the inactive state. The transaction between idle and connected states is slower, because there is neither RRC context nor CN connection in the idle state. The UE can move from the inactive to the idle state, but not vice versa. As can be observed from Figure 4, in the connected state, mobility is handled by the network, while in idle and inactive states, mobility is handled by the UE. [1]
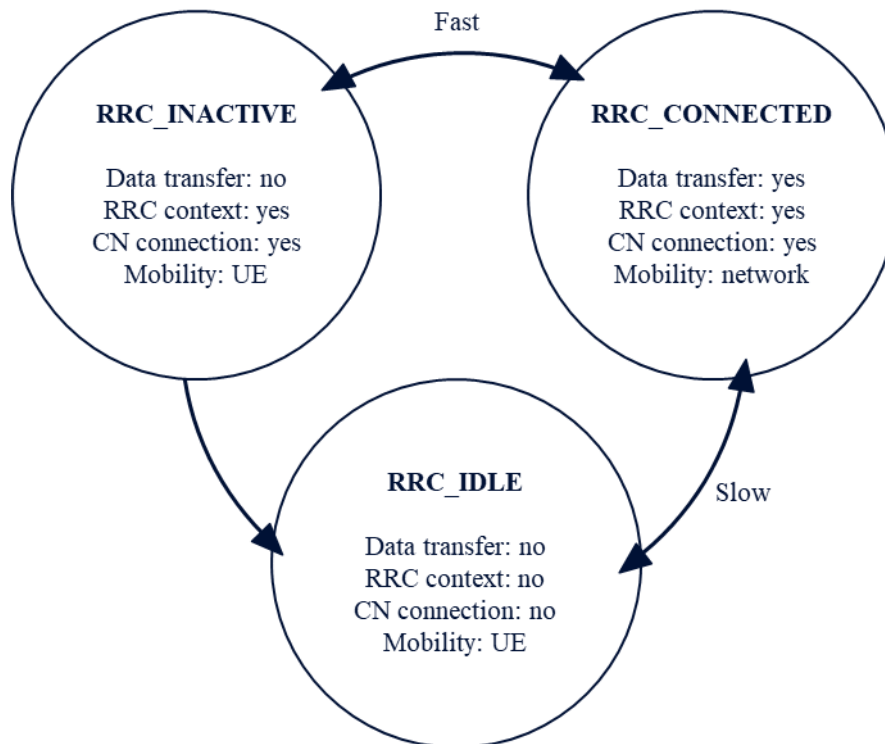
Figure 4. RRC state diagram of the NR.

While in the RRC_CONNECTED state, the UE is configured with one or more CORESETs. The UE monitors a set of PDCCH candidates within these CORESETs. Monitored PDCCH candidates are defined by PDCCH search space sets. The UE can monitor PDCCH according to one or more search space sets. Search space sets can be common or configured UE-specifically. Search space set parameters, like position, aggregation levels and the number of PDCCH candidates are configured by higher layer parameters between the UE and the cell. [14]

A failure in PDCCH reception causes the UE to lose the scheduled data transmission, while consecutive failures cause the UE to reselect another cell. The reselection of a cell is a costly procedure and affects the user's QoE negatively. So, the reliable reception of PDCCH is very important to ensure a stable operation of the network. [16]

After the traffic arrival, the UE stays in the connected state until the specified user-inactivity timer expiry to avoid excess latency from the RRC state transitions [22]. Since this procedure is done even if there is no upcoming traffic, it is a potential waste of energy [22]. According to the 3GPP, the target for the NR UE battery life for the mMTC usage scenario should be at least 10 years, and 15 years is desirable [23]. In LTE, over half of the UE's total power consumption comes from the connected mode [5]. So, it is important to study ways to decrease UE power consumption in the RRC_CONNECTED state [5]. UE operation in the connected mode, existing power saving techniques and the introduction of a new power saving signal are further discussed in Chapter 3.

3 UE POWER SAVING TECHNIQUES IN 5G NEW RADIO

This chapter provides an overview of existing power saving techniques, as well as possible operating principles and the design of a new technique, the UE power saving signal. Firstly, examples of existing power saving techniques in time and frequency domain are discussed. Then the last part of this chapter focuses on the properties and possible design options of the so-called UE power saving signal.

3.1 Time Domain

One example of UE power saving techniques in the time domain, is the usage of DRX. DRX is already used for example in LTE. DRX has two states, sleep and active (on-period), and the UE switches between them periodically. During the on-period, the UE checks whether it should be active or go to sleep. If the base station has data transmission for the UE, it keeps the RF module on to monitor PDCCH and receive the data. If there is no data transmission from the base station, the UE goes to sleep and turns off its radio interface. Because the UE cannot know exactly when it is supposed to receive data, DRX is basically a trade-off between power saving and delay [24]. [25]

As mentioned in Section 2.3, the DRX functionality is used also in the NR and the operating principle of the NR-DRX is the same to that of LTE [1]. In the NR, RRC can configure the DRX functionality to the UE's MAC entity. DRX affects the UE's PDCCH monitoring in the RRC_CONNECTED mode. If DRX is not configured, the UE monitors PDCCH continuously. If DRX is configured, the UE monitors PDCCH discontinuously. The DRX operation is controlled by the parameters configured by RRC. These parameters set durations of the DRX cycles, timers and on/off periods in milliseconds. [26]

It is very typical that if the UE is scheduled to either receive or transmit data, it will be scheduled again soon. For this reason, after the UE is scheduled, it stays in an active state for a while. The duration of this active state is controlled by the inactivity timer. It restarts every time the UE is scheduled and the UE stays awake while the inactivity timer is on. DRX has also a timer, which is used in the case of erroneous transport blocks. If the transmission was erroneous, the timer wakes up the UE when the g Node B (gNB) is most likely going to retransmit the data. [1]

A long DRX cycle is the basic operation cycle of the DRX. In the long DRX cycle, the UE has configured PDCCH monitoring occasions during the active (on) period after being scheduled (as described above), while rest of the time it keeps the RF module off. The long DRX cycle is suitable for most of the usage scenarios. However, some services may have regular transmissions, which are shortly followed by transmissions with very little activity. For these kinds of scenarios, such as voice over internet protocol (VoIP), a so-called short DRX cycle can be used in addition to the long DRX cycle. In the case of VoIP, the short DRX cycle can be configured to be for example 20 milliseconds, because it is usually the time between VoIP packets. This way, the short DRX cycle would handle VoIP packets and the long DRX cycle would handle longer periods of time. [1]

An illustration of the UE's operation without DRX, with a long DRX and with a long DRX cycle combined with a short DRX cycle is presented in Figure 5. In it, without the DRX functionality, the UE keeps the main RF parts on to monitor every PDCCH occasion and never enters to the power saving mode. The DRX cycles have the on-period to monitor PDCCH, and the sleep period for power saving. With the DRX functionality, if the UE is not scheduled during

the on-period, it switches to the power saving state for the rest of the DRX cycle. If the UE is scheduled during the on-period, it starts the inactivity timer and remains awake until the timer stops. After the timer stops, the UE continues the long DRX cycle normally, and if configured, starts the short DRX cycle. If the short DRX is configured, the UE follows short DRX cycles for a configured time, and in Figure 5 this time is presented by the short DRX timer. During the short DRX timer the UE has on-periods more often to monitor PDCCH occasions. Since the UE does not know when a new data transmission is coming unless it monitors PDCCH, the length of the DRX cycle determines the trade-off between power-saving and delay. When the short DRX cycle is configured, PDCCH is monitored more often, so the potential delay is less but the overall power consumption is higher. [1]

In addition to the DRX and the RRC configuration, the on duration can also be stopped in the middle by the gNB. In this way, the network can reduce UE power consumption, if the gNB knows that no additional data is awaiting downlink transmission. If the gNB instructs the UE to stop the on duration, it can instruct the UE to follow the long DRX cycle after termination. [1]
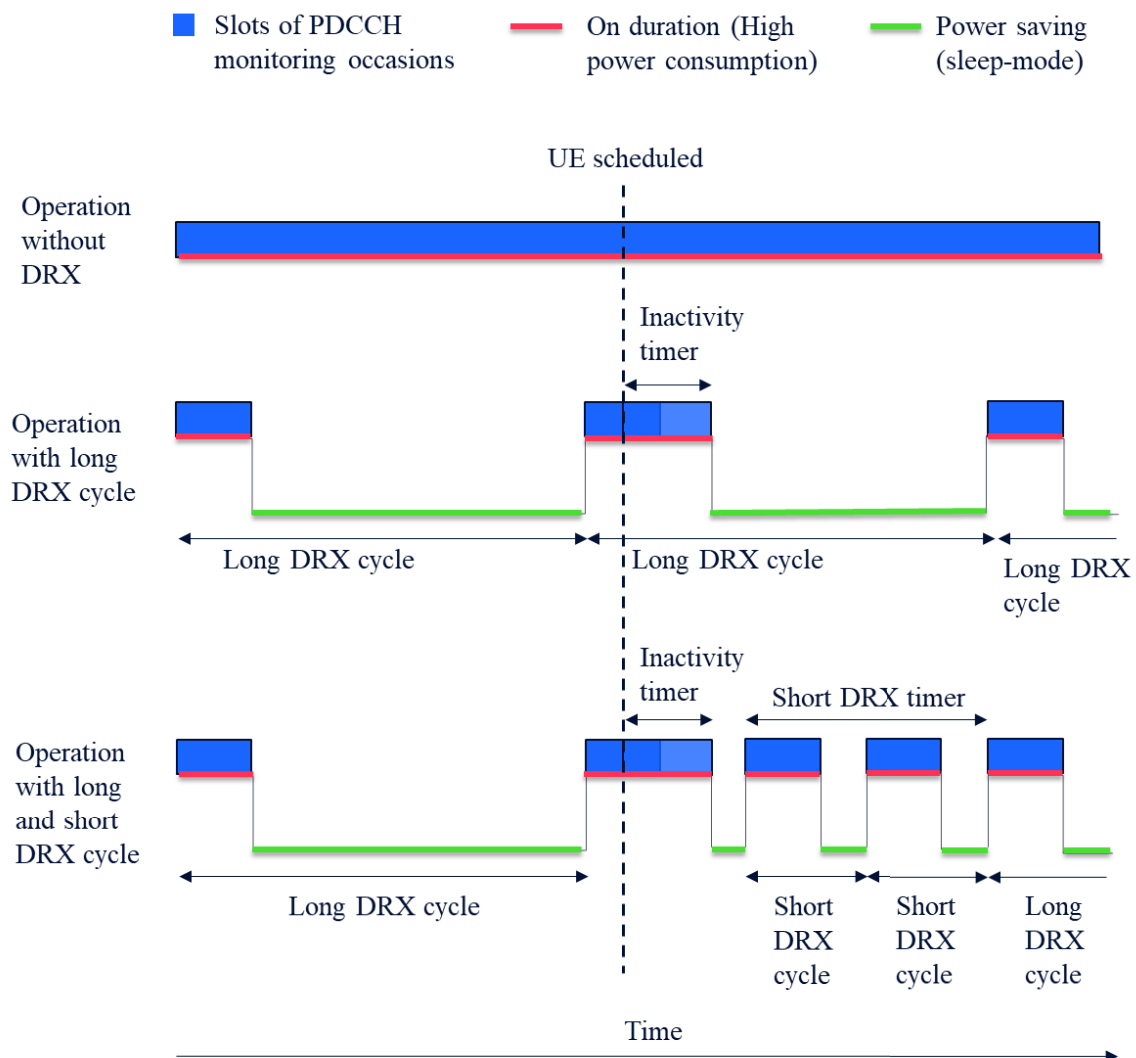
Figure 5. The UE's operation without DRX, with a long DRX cycle and with a long and a short DRX cycle.

3.2 Frequency Domain

To meet the requirements of high data rate and bandwidth, the NR supports a scalable subcarrier spacing and a wide carrier bandwidth (CBW). However, there are UEs that do not necessarily support the wide CBW, and high data rates are not required with every application. In such cases, the wide BW means higher idling power consumption in the RF and baseband parts. To improve energy efficiency in the frequency domain, the NR introduces a mechanism called a bandwidth part (BWP). The BWP framework provides a way to adaptively adjust UEs to operate with a smaller BW than the configured CBW, and the power saving is obtained with smaller BWPs. This way, the NR enables a simultaneous operation of wideband UEs and narrowband UEs. [27]

A demonstration of the BWP configuration in the frequency domain is presented in Figure 6. The total CBW is the size of the UE specific CBW in PRBs. BWP1, BWP2 and BWP3 demonstrate three example BWP configurations. As can be observed, BWP is either the size of the total CBW (BWP 3) or a piece of it (BWP 1 and 2), and it is composed of contiguous PRBs. The BWP cannot be wider than the CBW, and it must be at least as large as one SSB (20 PRBs). For a single UE, the network can configure up to four BWPs for the uplink and the downlink each. [27]
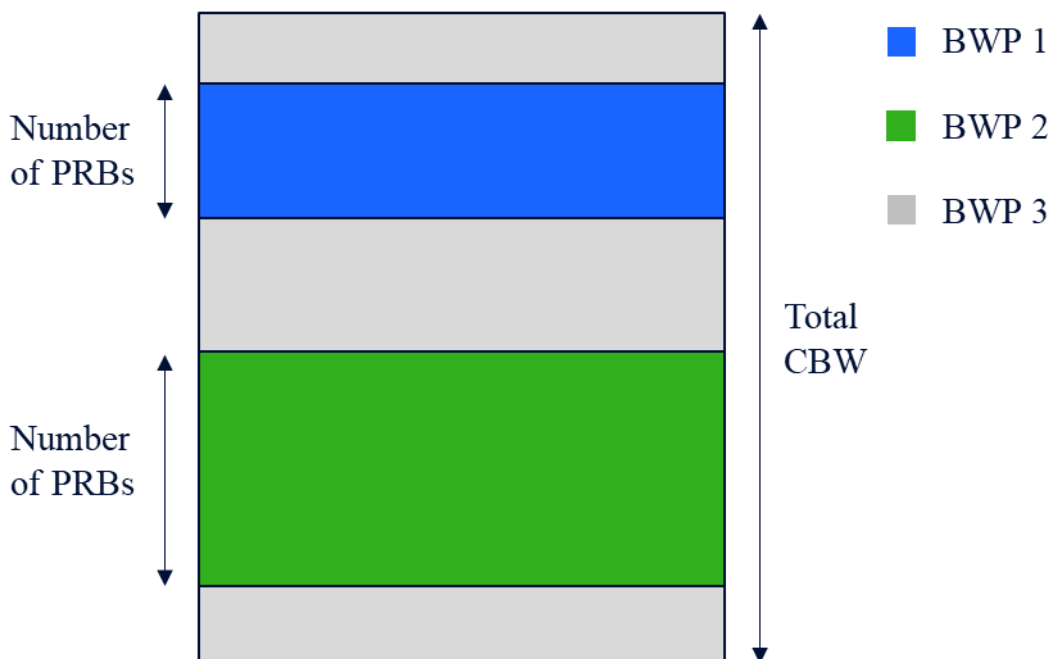

Figure 6. A demonstration of the bandwidth part configuration in the frequency domain.

3.3 UE Power Saving Signal/Channel

As described in Section 2.3, the PDCCH monitoring is seen as a very power-hungry operation. For that reason, the UE would benefit from a power saving mode, where the continuous PDCCH monitoring is not on. In the ideal case, the UE would monitor PDCCH only when it knows that the data transmission is coming. One way for a base-station to tell a UE whether it should monitor PDCCH or not, is to use a dedicated UE power saving signal/channel. The purpose of the UE power saving signal/channel is to reduce PDCCH monitoring, while the UE is in the

RRC_CONNECTED state. In this thesis, the UE power saving signal/channel is used in so-called wake-up and go-to-sleep scenarios. The wake-up/go-to-sleep mechanism, power saving potential, and the design of the power saving signal/channel are further analyzed in this section.

3.3.1   *Wake-up/Go-to-sleep Mechanism*

In the wake-up/go-to-sleep scenario, the UE has two possible modes during the DRX cycle. The first mode is the normal operation of the UE, described in Section 3.1, in which PDCCH is monitored periodically with the main RF module and the baseband parts switching on and off. The second mode is for power-saving (sleep-mode), where PDCCH is not monitored at all and the main baseband parts stay off during the whole DRX cycle. To switch between the sleep-mode and the normal mode, the base station can send wake-up or go-to-sleep information to the UE. The purpose of the wake-up/go-to-sleep mechanism is to reduce UE's power consumption by minimizing unnecessary PDCCH monitoring.

One way for a base station to trigger the UE to wake up from a sleep-mode to PDCCH monitoring, is to use a dedicated power saving signal/channel. The idea of the power saving signal/channel is that it can be received with a simple receiver that has a low power consumption. In this way, the power hungry main baseband and the RF parts can stay off during the whole DRX cycle. Because of the operation principle of this type of power saving signal/channel, it is called the wake-up signal (WUS) in this thesis. An illustration of the wake-up mechanism and the WUS operation is presented in Figure 7. Therein, at first the UE is in the sleep-mode during the DRX cycle and the main baseband parts are turned off. Then, the UE detects WUS with a simple detector and turns the main baseband parts on. After that the UE can detect the control information from PDCCH and thereafter receive the data from PDSCH.
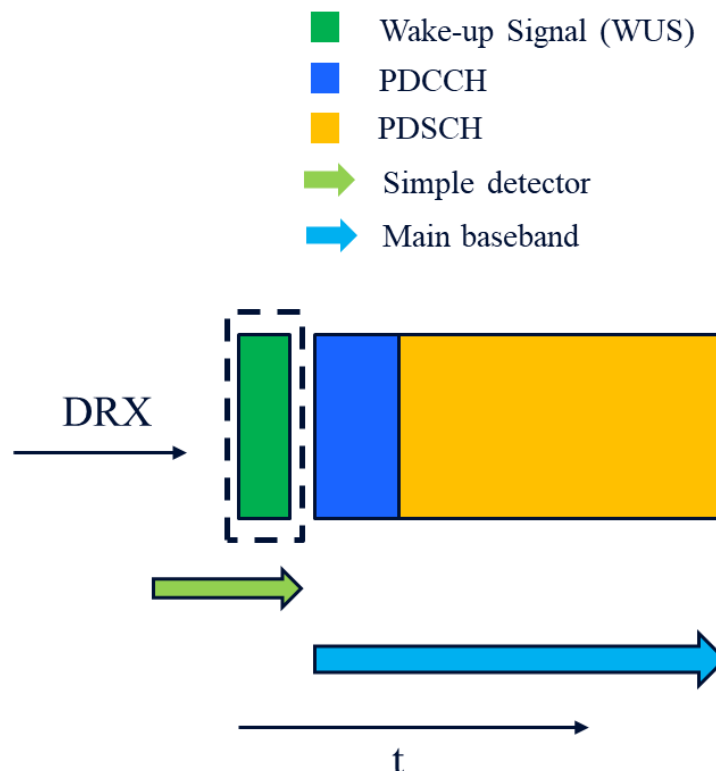

Figure 7. The wake-up mechanism and the WUS operation.

Normally, even though the UE has received all the data and there is no PDSCH transmission, the UE continues to monitor PDCCH. Despite of the fact, that UE can be configured to use DRX, it still must monitor PDCCH periodically, in the case of a new data transmission is scheduled for it. As mentioned in Section 3.1, in addition to the DRX and the RRC configuration, the on duration can also be stopped by the gNB. This operation can be described as go-to-sleep (GTS) signaling. With GTS, the gNB can inform the UE to stop PDCCH monitoring and switch to the sleep-mode, if there is no more data to transmit. The UE can wake up from the sleep mode, either during the next DRX cycle, or when it receives WUS. Therefore, the operation of WUS and GTS can be combined to achieve higher power saving potential. GTS can be based on the existing MAC-based command, or GTS could be carried by the same signal/channel as WUS. In the latter case, the UE power saving signal would have at least two different operation modes, wake-up and go-to-sleep. [5]

A comparison of the UE operation with and without DRX, as well as the operation with DRX and WUS is illustrated in Figure 8. Therein, without DRX or WUS, the UE never goes to the power saving state. This is the most power consuming option. The operation with DRX offers some improvements for power consumption. With DRX, the UE monitors PDCCH until the inactivity timer stops, and after that periodically. The long DRX cycle has less power consumption than the short DRX cycle, but on the other hand it has potentially more delay. In the lowest scenario in Figure 8, the UE is configured with DRX and WUS. In this scenario, WUS is transmitted in the configured WUS monitoring occasion. If the UE does not receive WUS, it can sleep during the on-period. If the UE receives WUS, it wakes up to monitor PDCCH in the on duration. In Figure 8, the UE goes to sleep after the inactivity timer expires, but it could also go to sleep in the middle of the on-period, if the on-period is terminated by the gNB with GTS signaling. With the WUS functionality, the UE has potentially smaller total power consumption, compared to the operation with DRX only. Hence, the WUS functionality would be a good addition to the NR, since it would improve power consumption compared to the operation with DRX only.
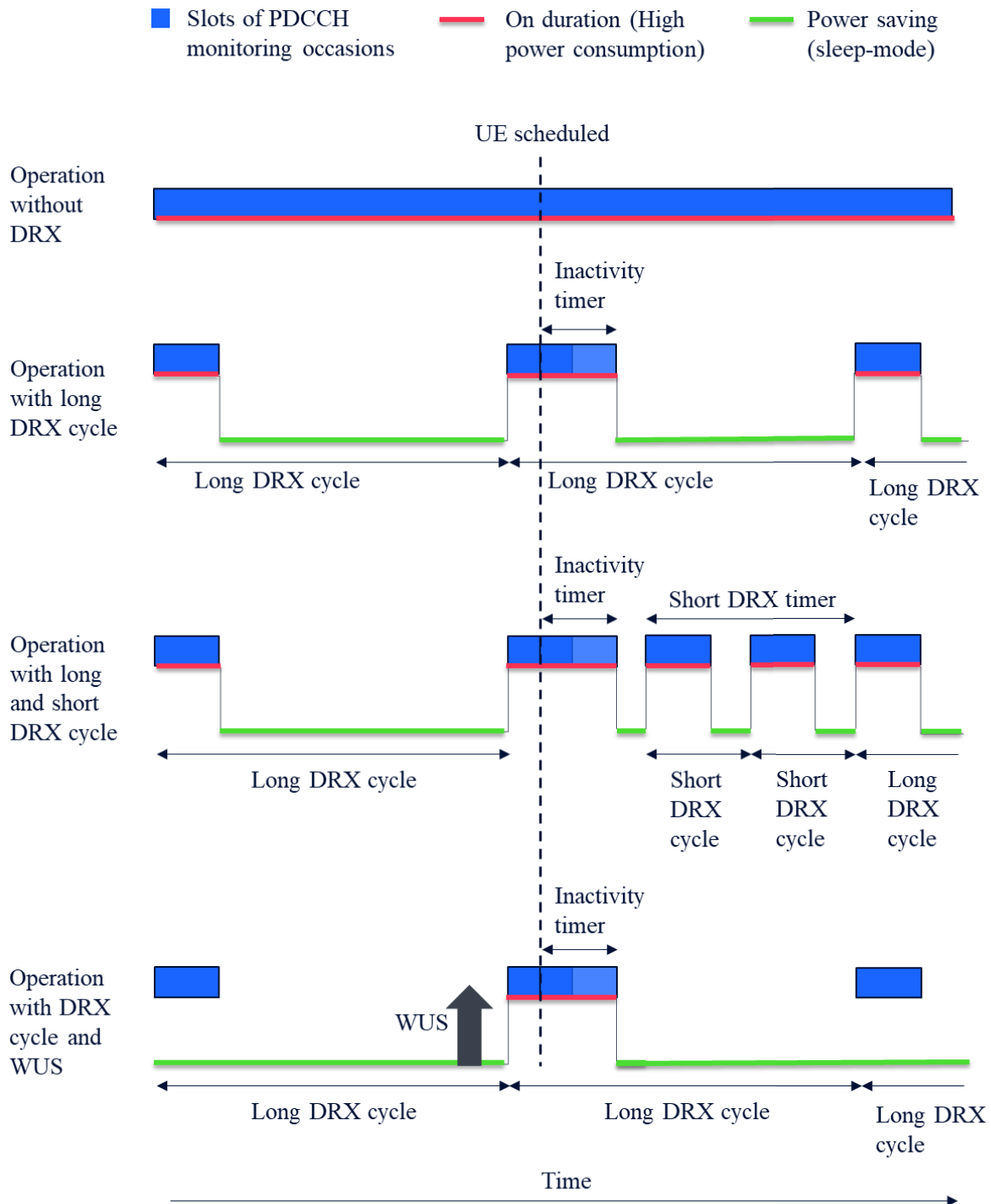
Figure 8. A comparison of the UE operation with/without DRX and with DRX and WUS.

3.3.2 *Power Saving Potential of the Wake-up/Go-to-sleep Mechanism*

The wake-up type operation in radio transceivers has been studied for other radio systems as well, for example with the institute of electrical and electronics engineers (IEEE) standard 802.11, commonly known as the wireless local area network (WLAN). In IEEE 802.11 standardization, the studied wake-up concept is called the wake-up radio. In the wake-up radio,

power saving is achieved by keeping the UE in the power saving state and waking it up with low-power wake-up signaling. IEEE estimates that power consumption in WLAN can be reduced by 94% with the low-power wake-up radio [28]. The wake-up radio is seen beneficial especially to the IoT and wireless sensor network applications, where power consumption and availability are big issues. [29]

Currently, the wake-up type power saving signal is a part of 3GPP study item "Study on UE Power Saving in NR". 3GPP technical report 38.840 [5], has evaluation results from the contributing companies, regarding the power saving scheme of power saving signal/channel triggering the UE adaptation to the DRX operation. In the evaluation assumptions, the power saving signal/channel wakes the UE up for PDCCH monitoring, if there is a downlink data arrival for the UE. The UE does not wake up if it is not triggered by the wake-up signal/channel. GTS signaling is used to indicate whether the UE should switch to the sleep-mode after the PDSCH reception. [5]

Based on the evaluations, the wake-up triggering power saving signal provides 8% - 50% power saving gain, compared to the normal DRX configuration. The relative power saving gain depends heavily on the reference case, so the dispersion of the potential power saving gain is large. With a longer DRX cycle and/or high traffic load, the gain is typically 5% - 10%, but with a shorter DRX cycle, the gain is larger. Especially, the length of the DRX cycle and the on duration impacts the relative power saving gain. This is logical, since the UE have more on-periods with the short DRX cycle, and WUS can decrease the number of needless on-periods. Based on the evaluations, the WUS/GTS operation causes latency increase in the range of 2%-13% and the user perceived throughput degradation in the range of 0.5%-16%. The power consumption level of the power saving signal/channel has only a minor impact on the achievable power consumption. Therefore other aspects, such as the detection performance, play an important role in the design. [5]

An illustration of the impact of the DRX configuration to the potential power saving achieved with WUS is provided in Table 3. The results and DRX schemes of Table 3 are from the 3GPP contribution R1-190313 [30]. Table 3 compares the achieved power saving of the two DRX configuration cases. The first case has only the long DRX cycle configured, and the other case has the long DRX cycle combined with the short one. As evident, with these configurations, the relative power saving is over two times larger when the short DRX cycle is used. [30]

Table 3. The impact of the DRX configuration to the potential power saving achieved with WUS.

Case	Only long DRX cycle	Long DRX cycle combined with short DRX
Long DRX cycle duration	160 ms	80 ms
Short DRX cycle duration	-	40 ms
Number of short cycles	-	3
Relative power saving achieved with WUS	7.8% - 8.6%	18.6% - 20.3%

3.3.3   UE Power Saving Signal Design

Since the 5G-NR currently does not have wake-up/go-to-sleep type of operation, the design of the UE power saving signal, in this case the wake-up signal, could be based on a completely new signal. However, the NR already has potential signals and channels, which could be reused/configured as WUS. By utilizing the existing signals/channels, the UE can use the same RF parts as it uses already, and the complexity of the overall design is not unnecessarily increased. In this thesis, the existing NR physical layer signals and channels are studied and evaluated to be used as the UE power saving signal (WUS). The evaluated channels and signals are based on 3GPP Release 15 and five signal/channel structures are studied for the WUS usage. The baseline for the studied candidates is the 3GPP technical report 38.840 [5].

The candidates are presented in Table 4. It has listed basic time and frequency structure of the candidates, as well as the type and the total number of REs. Basic properties of the signals and channels are described in more detail in Section 2.2. As illustrated in Table 4, the WUS candidates of this work can be divided into three categories based on their type. Three types are the frequency domain sequence, the time domain sequence and the regular PDCCH. WUS options are discussed in detail below and the properties of the WUS detectors/receivers are described in Section 4.1.

The frequency domain sequence means a sequence, which can be detected at the receiver with a simple correlator, in the frequency domain. Three frequency domain sequence options for WUS are studied. In Option 1, the WUS design is based on the SSS sequence. Like SSS, Option 1 consists of the length 127 Gold sequence, which is mapped to one OFDM symbol in time and 127 continuous subcarriers/REs in the frequency domain, as described in Section 2.2.2.

In Option 2, the WUS design is based on the PDCCH DMRS sequence. This means that Option 2 consists of the UE specific QPSK pseudo-random sequence, which is mapped to each fourth subcarrier of PRBs. Option 2 is studied with 6, 12, 24, 48 and 96 PRBs, which corresponds to the aggregation levels 1, 2, 4, 8 and 16. Therefore, the total number of REs in Option 2 is $3N_{PRB}$, where N_{PRB} is the number of PRBs.

In Option 3, the design of the WUS is based on the CSI-RS/TRS sequence. Option 3 consists of the QPSK pseudo-random sequence, just like Option 2, but with a different initialization value. Option 3 consists of two OFDM symbols in time, which are four symbols apart, as described in Section 2.2.5. In the frequency domain, Option 3 consists of 48 contiguous PRBs per OFDM symbol. The sequence is mapped to each fourth subcarrier of the PRBs. Therefore, the total number of REs in Option 3 is 288.

In Option 4, the UE uses a simple time-domain correlator for the WUS detection. This means that the correlation between the received signal and the reference WUS is done between time domain signals. The sequence of the option four is based on PDCCH DCI. Option 4 is studied with 6, 12, 24, 48 and 96 PRBs, which corresponds to the aggregation levels 1, 2, 4, 8 and 16. In this scenario, the sequence is a UE specific QPSK sequence, which is mapped to every subcarrier of PRBs, including subcarriers that normally would carry PDCCH DMRS. Therefore, the total number of REs in Option 4 is $12N_{PRB}$, where N_{PRB} is the number of PRBs.

In Option 5, the design of the WUS is based on the regular PDCCH. In this scenario, the regular PDCCH is used as to carry the wake-up indication/information as the payload of the DCI. In this work, the payload of the PDCCH is set to 34 bits (10 data bits + 24 CRC bits), except in Section 5.4, where different payload sizes are compared. This design utilizes all the properties of the regular PDCCH transmission, including polar encoding, precoder cycling and

the estimation of the PDCCH-DMRS. The CORESET size is set to 96 PRBs, and the aggregation levels 6, 12, 24, 48 and 96 are studied.

Table 4. The candidate wake-up signals/channels and their properties.

Option	Signal/ channel	Type	PRBs	Symbols	Total number of REs
1	SSS	Frequency domain sequence	12	1	127
2	PDCCH DMRS	Frequency domain sequence	6/12/24/48/96	1	18/36/72/144/288
3	CSI-RS / TRS	Frequency domain sequence	48	2	288
4	PDCCH DCI + DMRS	Time domain sequence	6/12/24/48/96	1	72/144/288/ 576/1152
5	PDCCH	Regular PDCCH channel	6/12/24/48/96	1	72/144/288/ 576/1152

4   SIMULATION MODELLING

In the simulations of this work, candidate signals/channels for WUS are studied with link-level simulations. Numerical results are evaluated in terms of the detection performance. Numerical results of the simulations are presented in Chapter 5. This chapter describes the operation of the used simulator, as well as the used simulation parameters and simulation cases.

4.1   Detection Performance and Simulator Structure

A Matlab-based link-level simulator was used in the simulations of this thesis. Matlab is a matrix-based computing language and desktop environment, suitable for computational mathematics [31]. A block diagram of the simulator's transmitter (TX) branch and channel is presented in Figure 9. At first, a set of WUS data/sequences is generated and one of them is used as a UE specific WUS. Then, the data/sequence is modulated and mapped to the allocated REs. After that, the data/sequence is converted from the frequency domain to the time domain using the inverse fast Fourier transform (IFFT). Lastly, the cyclic prefix is added and the WUS is sent through the channel. Channel models are described in Section 4.2 and a more detailed description of common simulation parameters is given in Section 4.3.
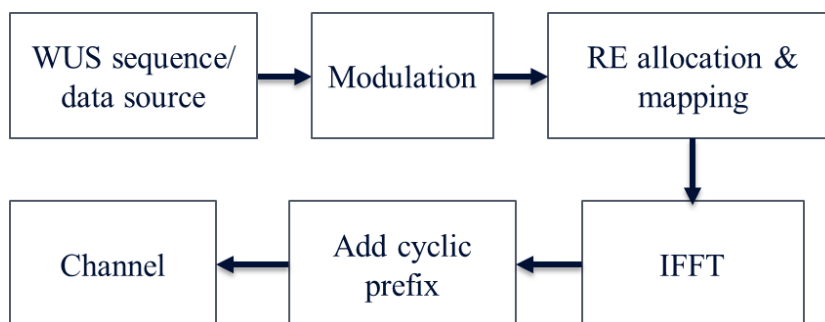
Figure 9. A block diagram of the simulator's transmitter branch and channel.

In this work, the detection performance is measured as a probability of miss-detection (PMD). PMD is the probability that the UE does not detect (miss) the WUS transmission when it is sent. A false alarm is an event, where the receiver detects a correct WUS, even though the WUS is not actually transmitted. Probabilities are presented as values between 0 and 1, where 1 corresponds to 100 % probability and 0 corresponds to 0 % probability.

As discussed in Section 3.3.3, five candidate signals/channels for the WUS are studied in this work. Options are either based on the frequency domain sequence, the time domain sequence or the regular PDCCH. Because of that, the simulator has different RX branches for sequence based and PDCCH based transmissions. In these simulations, every branch assumes ideal timing.

A block diagram of the simulator's sequence detector is presented in Figure 10. If the WUS is based on the time domain sequence, the signal is collected into a vector without a fast Fourier transform (FFT). If the WUS is based on the frequency domain sequence, it is firstly transformed to the frequency domain using FFT and then the signal is collected into a vector. After that the detector works similarly for all the sequences. The signal vector is firstly correlated with all the known candidate signal vectors. Correlation results are then compared to the threshold value. If the correlation result is lower or equal than the threshold value, the detector draws a conclusion that only the noise is received. If the WUS is transmitted, but the

detector fails to detect it, this occasion is interpreted as a miss-detection. If the correlation result is higher than the threshold value, the detector draws a conclusion that the signal is detected. If the detected signal is the correct transmitted WUS, this occasion is interpreted as a correct detection (hit).

If the signal is detected, but it is not the correct transmitted WUS, this occasion is interpreted as a false alarm. The threshold is determined a per sequence set so that the false alarm against just the noise is 1%. To determine the false alarm against the noise, the simulator's transmitter alternates between the WUS transmission and no transmission at all. So, between every WUS transmission, the detector receives only the noise from the channel. This way, the false alarm against the noise can be determined to every signal-to-noise ratio (SNR) value, individually as an offline processing.
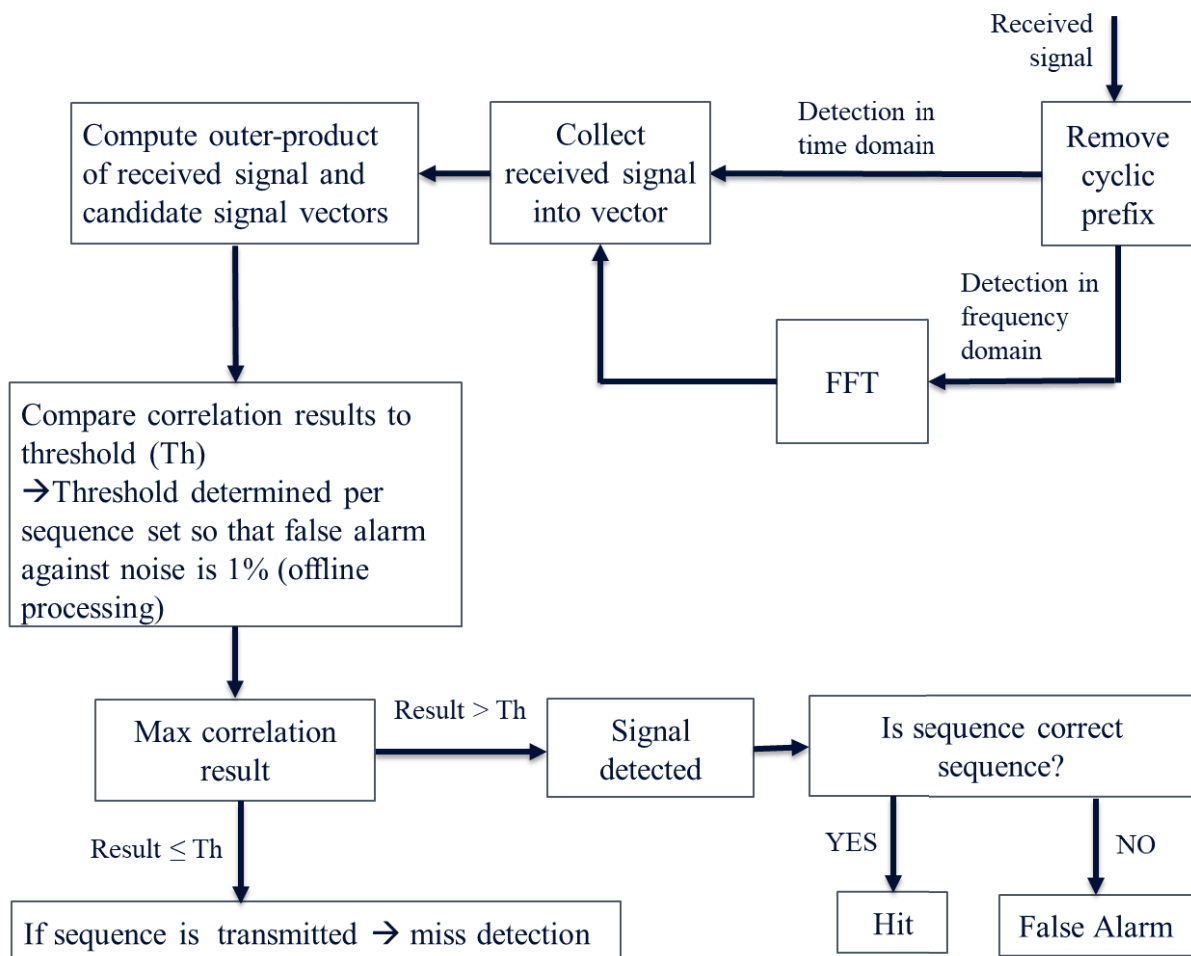
Figure 10. A block diagram of the simulator's sequence detector.

As mentioned in Section 3.3.3, the PDCCH based WUS (Option 5) utilizes all properties of the regular PDCCH transmission. Because of this, the detection of Option 5 is a little more complex than the detection of the sequence-based options. At first, CP is removed and then the signal is transformed to the frequency domain using FFT. After that, the receiver estimates the channel based on the available information from DMRSs. Then, the receiver uses channel estimates to equalize the received signal. Lastly, signal is demodulated, decoded and CRC check is performed. If the CRC check result is correct, receiver draws a conclusion that data is

received correctly. If the transmitted data is received correctly, this is interpreted as a correct detection. If not, this is interpreted as a miss-detection.

4.2   Channel Models

Simulations in this thesis use additive white Gaussian noise (AWGN) as a reference channel model and tapped delay line (TDL) models to represent channels with multipath fading conditions. In the AWGN model, the receiver's thermal noise is the main noise source. The thermal noise tends to have a flat power spectral density over the whole bandwidth and a zero-mean Gaussian voltage probability density function. Noise samples of the AWGN channel are statistically independent and the AWGN channel does not suffer from inter-symbol interference (ISI). [32]

The coherence bandwidth $(\Delta f)_\text{c}$ of the channel is defined by

$$(\Delta f)_\text{c} \approx \frac{1}{T_\text{m}}, \tag{24}$$

where T_m presents the multipath spread of the channel. If the bandwidth of the information-bearing signal is larger than the coherence bandwidth, the channel is seen as frequency-selective. If the bandwidth of the signal is smaller than the coherence bandwidth, the channel is seen as non-frequency-selective. The frequency-selective channel heavily distorts the transmitted signal, because the attenuation and the phase shift are different between frequency components. In the non-frequency-selective channel all frequency components undergo the same attenuation and phase shift. [33]

The coherence time $(\Delta t)_\text{c}$ of the channel is defined by

$$(\Delta t)_\text{c} \approx \frac{1}{B_\text{D}}, \tag{25}$$

where B_D is the Doppler spread of the channel. If the signaling time of the information bearing signal is larger than the coherence time, the channel is called a fast fading channel. If the time of the signal is smaller than the coherence time, the channel is called a slow fading channel. Fading means an additional variation in the strength of the received signal. The fast fading channel causes distortion to the strength of the transmitted signal, because of the channel's variation during the transmission. In the slow fading channel, the attenuation of the signal strength stays relatively constant during the transmission, assuming that the transmission is served as relatively short bursts. [33]

The fading multipath channel causes an extra penalty to the SNR of the signal. Fading effects are further divided into two categories, large-scale and small-scale fading. Large-scale fading represents the average signal power attenuation over large areas and is affected by the obstacles between the transmitter and the receiver, such as buildings, forests or hills. Small-scale fading represents rapid and significant changes in the signal amplitude and phase and is affected by small changes in spatial separation between the transmitter and the receiver. Rayleigh fading is a type of small-scale fading, without the line of sight component but with many reflective paths that follow the Rayleigh probability distribution function.

3GPP has specified five TDL channel profiles, which represent different channel environments. TDL-A, TDL-B and TDL-C are non-line of sight (NLOS) channel profiles, while TDL-D and TDL-E are line of sight (LOS) channel profiles [34]. All NLOS profiles have a Rayleigh fading distribution, while LOS profiles have a Rician fading distribution in the first tap and a Rayleigh fading distribution in the rest of the taps. Profiles can be scaled in delay, to achieve a desired root mean square (RMS) delay spread. The Doppler spectrum for each tap has the Jakes spectrum shape and the maximum Doppler shift f_D is defined by

$$f_D = \frac{|\bar{v}|}{\lambda_0},$$ (26)

where $\bar{v}$ is velocity and λ_0 is the wavelength. [34]

In this work, three channel models, AWGN, TDL-A and TDL-C have been used in the simulations. AWGN results present the optimal conditions and work as a reference point to the fading channel model. TDL channel profiles have different environments and usage scenarios. TDL-A presents an indoor hotspot in an isolated environment, such as an office or a shopping mall, with a very high density of pedestrian and stationary users. TDL-C presents a large rural environment with pedestrian, vehicular and high-speed vehicular users. [35]

As mentioned before, TDL-models can be scaled in delay. RMS delay spreads of the simulation's TDL-models are chosen so that they correspond to different frequency-selectivity properties. The RMS delay spread of TDL-A is very short (30 ns), so the channel is not very frequency selective. TDL-C is simulated with two RMS delay spreads, 100 and 300 ns. 100 ns is a nominal delay spread, so the channel is already somewhat frequency selective. 300 ns delay spread is long, so the channel is very frequency selective. [34]

4.3   Simulation Cases and Parameters

In Section 3.3.3, five candidate signal/channel types for the WUS were presented. Simulations in this thesis compare the detection performance of these five options in different conditions. Simulation cases include impacts of channel conditions, subcarrier spacing, carrier frequency offset (CFO) and UE speed. As the basis for the common simulation parameters are the simulation assumptions specified in Table A.1.5-1 in the 3GPP Technical Report 38.802 [20]. Used simulation parameters are presented in Table 5. 4 GHz carrier frequency and two TX/RX antennas are used in all cases. SSS-based WUS (Option 1) uses binary phase shift keying (BPSK) and the rest of the options use QPSK. CSI-RS/TRS-based WUS (Option 4) has two OFDM symbols in time, as presented Section 2.2.5 and the other options have one symbol in time.

WUS options are simulated with and without 400 Hz carrier frequency offset and with subcarrier spacings 15 and 30 kHz. Used channel models are AWGN, TDL-A with 30 ns RMS delay and TDL-C with 100 and 300 ns RMS delay spreads. Channel models are described with more details in Section 4.2. Two UE speeds were studied, 3 km/h and 120 km/h. The last row of Table 5 describes the length of the simulations. 30000 samples per SNR point means that the simulator calculates 30000 PMD samples per SNR point, and the resulting probability is the mean of those samples.

Table 5. Common simulation parameters.

Parameter	Value
Carrier frequency	4 GHz
Carrier frequency offset	0 & 400 Hz
Subcarrier spacing	15 & 30 kHz
Modulation	BPSK in SSS, QPSK in others
Channel	AWGN, TDL-A 30 ns, TDL-C 100 ns & TDL-C 300 ns
Number of TX/RX antennas	2/2
UE speed	3 km/h & 120 km/h
OFDM symbols	2 in CSI-RS/TRS, 1 in others
Number of samples in the simulation	30000 / SNR point

5 DETECTION PERFORMANCE SIMULATION RESULTS

In this chapter, the detection performance of the candidate WUS options is studied based on the numerical results from the link level simulations. The focus of this chapter is to study the impact of frequency- and time-selectivity, as well as the impact of the implementation impairments. Numerical results compare the detection performance of the WUS candidates with different channel models, UE speeds, subcarrier spacings and carrier frequency offsets. Numerical results are evaluated in terms of the probability of miss-detection (PMD) as a function of the signal-to-noise ratio (SNR). In this work, the target probability of miss-detection is $\leq 0.1\%$ at $\leq$ -4 dB SNR.

5.1 Impact of the Frequency-Selectivity

In this section, the impact of the frequency-selectivity is studied. As mentioned in Section 4.2, TDL-A 30 ns is not very frequency-selective, TDL-C 100 ns is somewhat frequency-selective and TDL-C 300 ns is a very frequency-selective channel. The AWGN channel works as a baseline for the comparison. Numerical results of all options, (with every AL in the case of Options 2, 4 and 5) in these channels are provided in this section. The subcarrier spacing is 15 kHz, the UE speed is 3 km/h and the carrier frequency offset is 400 Hz in every simulation of this section.

The detection performance of the SSS sequence based WUS (Option 1) in AWGN, TDL-A 30 ns, TDL-C 100 ns and TDL-C 300 ns channels is presented in Figure 11. As can be seen, in the AWGN channel, SSS reaches 0.1% PMD at -4.5 dB SNR, but the performance of the SSS is over 10 dB worse in fading channels. In TDL-A 30 ns and TDL-C 100 ns channels, SSS reaches 0.1% PMD at 8 dB SNR. However, in a very frequency-selective channel TDL-C 300 ns, SSS has 2.5 dB worse performance at 1% PMD, compared to the other fading channels. Therefore, SSS is sensitive to the very frequency-selective channel. Based on Figure 11, Option 1 achieves the target 0.1 % PMD at <-4 dB SNR only in the AWGN channel.
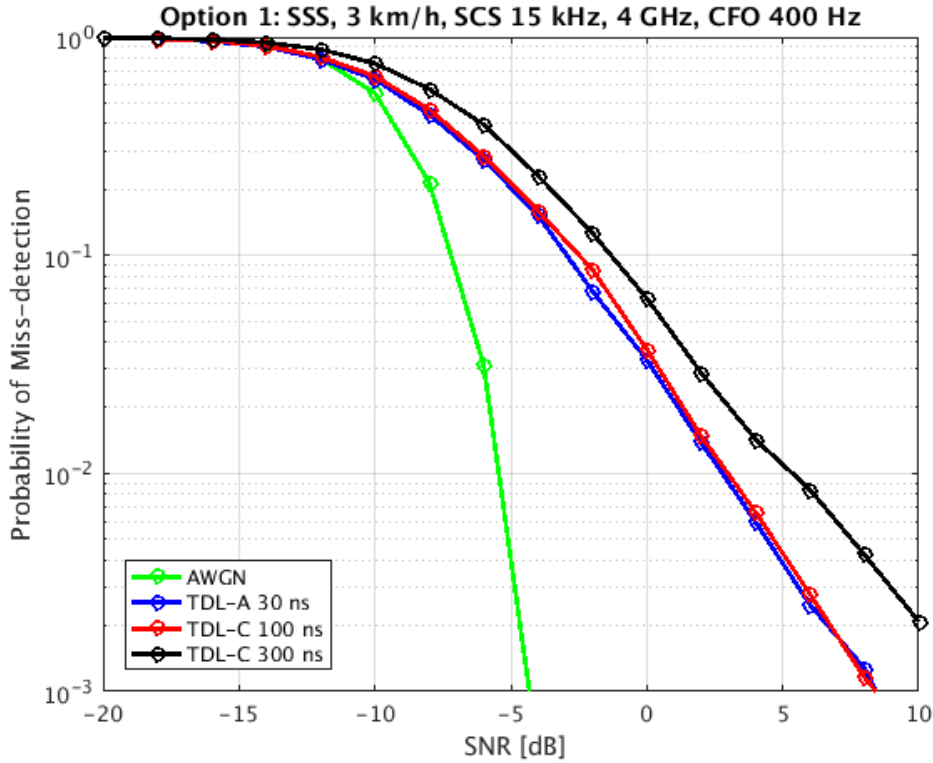
Figure 11. Option 1 (SSS) in AWGN, TDL-A 30 ns, TDL-C 100 ns & TDL-C 300 ns channels.

The detection performance of the Option 2 (PDCCH DMRS) in the AWGN channel is presented in Figure 12. It has PDCCH DMRS sequences of size 6, 12, 24, 48 and 96 PRBs, which correspond to aggregation levels 1, 2, 4, 8 and 16. Therein, doubling the number of PRBs improves the SNR by 3 dB. When compared to Figure 11, the PDCCH DMRS sequence with AL-8 has almost the same performance as the SSS sequence in the AWGN channel. At 0.1% PMD, the AL-8 DMRS sequence has only 1 dB better SNR than the SSS sequence. This is logical, since PDCCH DMRS AL-8 has 144 REs, while SSS has 127 REs, and there is no fading or ISI in the AWGN channel causing distortion. In the AWGN channel, Option 2 reaches the target SNR at 0.1% PMD with AL-8 at -6 dB and with AL-16 at -9.5 dB.

Option 2 with all ALs and without precoder cycling in TDL-A 30 ns, TDL-C 100 ns and TDL-C 300 ns channels is presented in Figure 13. As can be seen, with every AL, PMD is the best in the TDL-A channel with a short delay spread (30 ns). In the TDL-C channel with a nominal delay spread (100 ns), the SNR is <1 dB worse with ALs 1, 2 and 4, 2 dB worse with AL-8 and 3 dB worse with AL-16. In the TDL-C channel with a long delay spread (300 ns), the PMD performance drops dramatically, and the curves start to saturate to the final PMD value between 1-5%. As can be observed from Figure 13, with this configuration Option 2 does not achieve the target PMD at <-4 dB SNR with any AL.

As discussed in Section 2.2.3, the PDCCH DMRS sequence can utilize precoder cycling to achieve frequency diversity and thus better detection performance. In this work, the precoder cycling granularity is 6 PRBs, meaning that the precoder changes cyclically between every 6 PRBs. With precoder cycling, the sequence detector is also modified so that the decisions are made in 6 PRB wide frequency parts, which are then combined across the whole band. As mentioned in Section 4.2, the coherence bandwidth is smaller in the frequency-selective channels and simulation results show that in many cases, PMD starts to saturate in frequency-

selective channels. The idea of combining smaller frequency parts across the whole band is to ensure that the decisions are made within the channel's coherence bandwidth.

Option 2 with precoder cycling and frequency parts combining in TDL-A 30 ns, TDL-C 100 ns and TDL-C 300 ns channels is presented in Figure 14. As it turns out, with the precoder cycling and frequency parts combining, the PDCCH DMRS sequence becomes much more resistant to the frequency-selective channel. When compared to Figure 13, the curves with higher ALs no longer saturate to a final PMD and the graphs descend more steeper overall. With precoder cycling and frequency parts combining, the AL-16 case reaches 0.1% PMD between -3 and -5 dB in all fading channels, including TDL-C 300 ns. The detector clearly benefits from frequency diversity of precoder cycling and frequency parts combining, which results to higher gain. For that reason, these techniques are used by default in every following PDCCH DMRS simulation of this work.
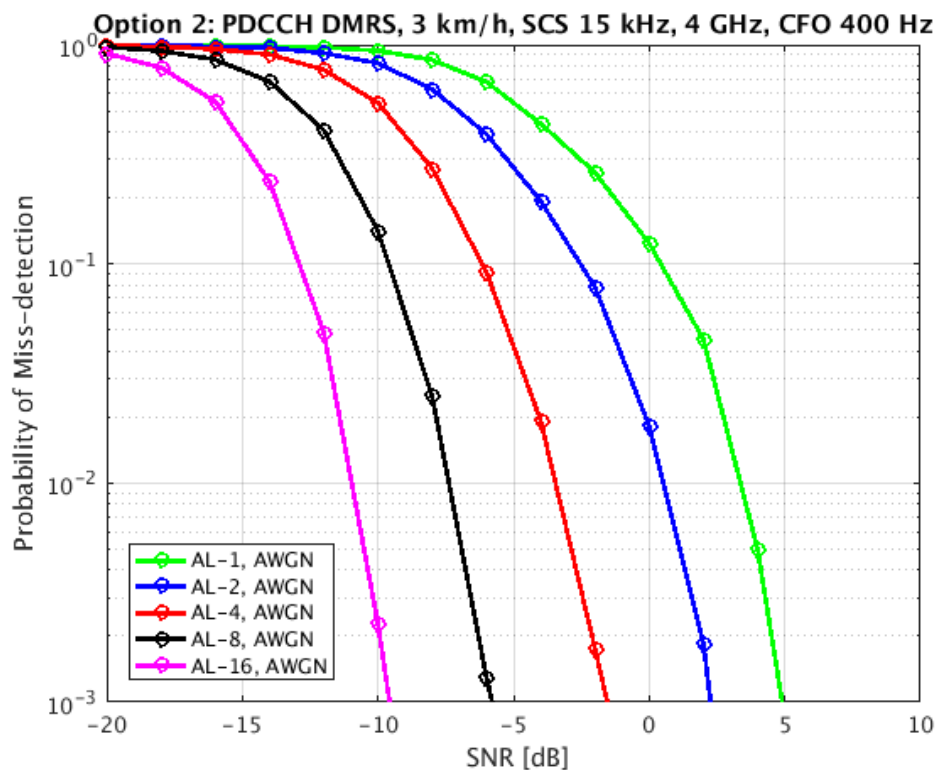
Figure 12. Option 2 (PDCCH DMRS) in the AWGN channel.
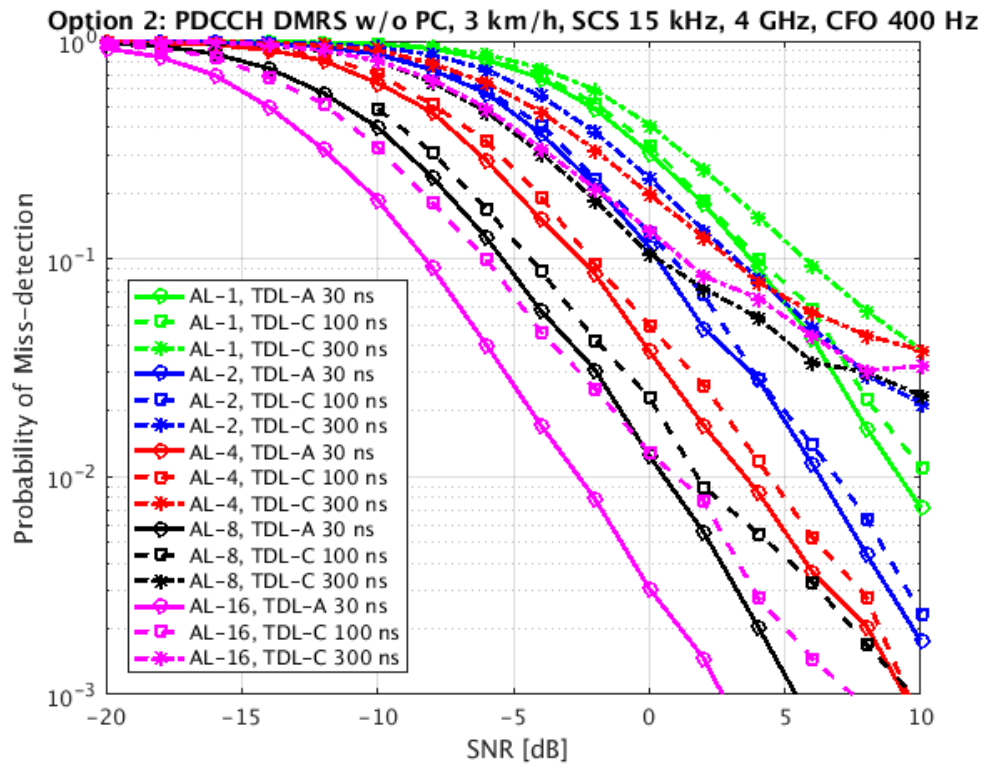
Figure 13. Option 2 (PDCCH DMRS) without precoder cycling in TDL-A 30 ns, TDL-C 100 ns and TDL-C 300 ns channels.
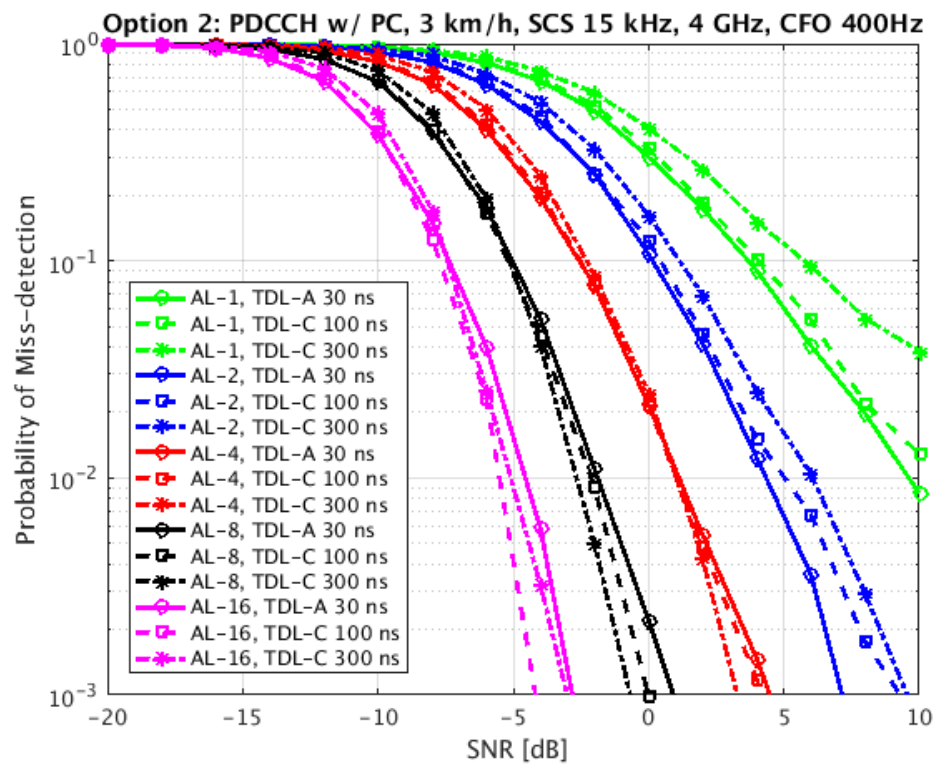
Figure 14. Option 2 (PDCCH DMRS) with precoder cycling in TDL-A 30 ns, TDL-C 100 ns and TDL-C 300 ns channels.

Option 3 (CSI-RS/TRS) in AWGN, TDL-A 30 ns, TDL-C 100 ns and TDL-C 300 ns channels is presented in Figure 15. Option 3 reaches 0.1% PMD at -8 dB SNR in the AWGN channel, at 2.5 dB SNR in the TDL-A 30 ns and at 8 dB SNR in the TDL-C 100 ns channel. In the TDL-C 300 ns channel, at 10 dB SNR, Option 3 has saturated to approximately 1% PMD, so Option 3 suffers from frequency-selectivity too.

The detection performance of the CSI-RS/TRS based WUS is comparable to the AL-16 PDCCH DMRS sequence based WUS. Both have 288 REs long QPSK pseudo-random sequences, but with different initialization values. The CSI-RS/TRS sequence is mapped to two OFDM symbols, while the PDCCH DMRS sequence is mapped to only one symbol. These reasons cause a slight difference between their performance. When comparing Figure 15 below to Figures 12 and 13 above, it can be observed that in AWGN and TDL-A 30 ns channels, at 1% and 0.1% PMD values, Option 3 has approximately 1-1.5 dB worse SNR than Option 2 (AL-16 case). In the TDL-C 100 ns channel, at 1% and 0.1% PMD, Option 3 has 1-2 dB better SNR than Option 2 (AL-16 case). In the TDL-C 300 ns channel, at 10% PMD, Option 3 has 3 dB better SNR than Option 2 (AL-16 case) and at 10 dB SNR, Option 3 saturates to 1% PMD, while Option 2 saturates to 3%. However, when compared to Option 2 with precoder cycling (Figure 14 above), it can be observed that Option 3 has over 5 dB worse SNR at 0.1% PMD in all fading channels.

When comparing Option 3 to Option 1 (Figure 11), at 0.1% PMD Option 3 has 3.5 dB better SNR in the AWGN channel. In the TDL-A 30 ns channel, at 1% and 0.1% PMD, Option 3 has 5 dB better SNR. In the TDL-C 100 ns channel at 1% PMD, Option 3 has 3.5 dB better SNR, but in 0.1% PMD, the SNR is approximately the same, because of the saturation of Option 3. In the TDL-C 300 ns channel, below 2 dB SNR, Option 3 has better PMD, but above 3 dB SNR, Option 1 has better PMD, because of the saturation of Option 3.
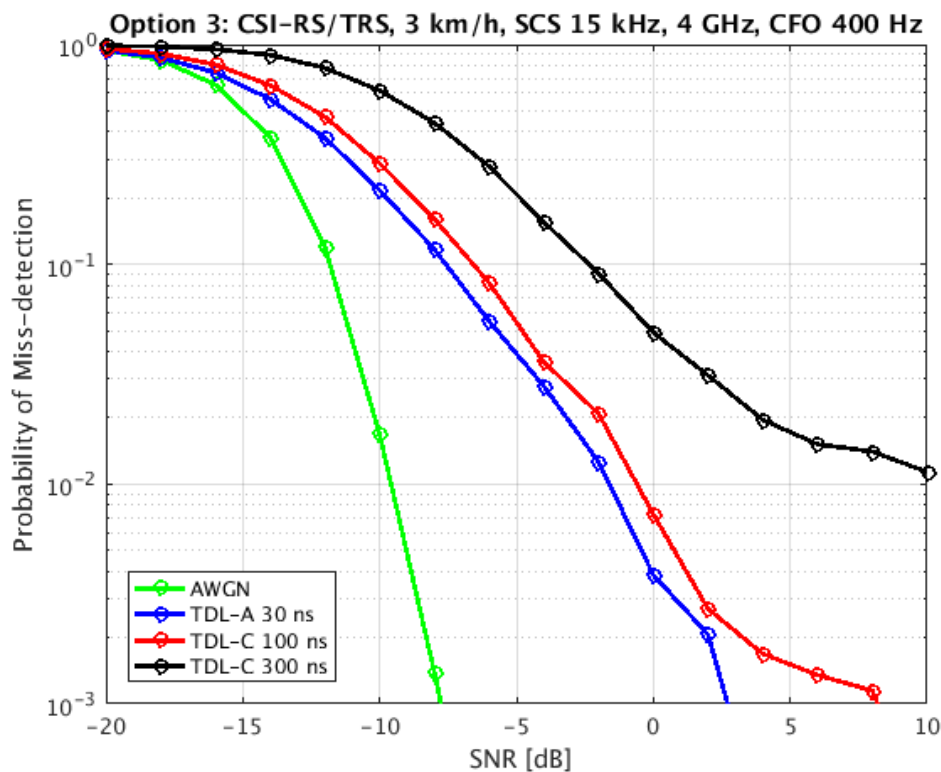

Figure 15. Option 3 (CSI-RS/TRS) in AWGN, TDL-A 30 ns, TDL-C 100 ns and TDL-C 300 ns channels.

The detection performance of Option 4 (PDCCH DCI+DMRS) with all ALs in the AWGN channel is presented in Figure 16. Option 4 in TDL-A 30 ns, TDL-C 100 ns and TDL-C 300 ns channels is presented in Figure 17. Figures 16 and 17 have sequences of size 6, 12, 24, 48 and 96 PRBs, which correspond to aggregation levels 1, 2, 4, 8 and 16. As can be seen from Figure 16, in the AWGN channel Option 4 reaches the target 0.1% PMD at <-4 dB SNR with aggregation levels 2, 4, 8 and 16. However, as can be observed from Figure 17, Option 4 does not reach the target PMD in fading channels with any AL. So, even though Option 4 with AL-16 has the best detection performance in the AWGN channel, it cannot compete with AL-16 Option 2 in frequency-selective fading channels.

In fading channels, PMD is the best in the TDL-A 30 ns channel. Compared to the TDL-A 30 ns channel, Option 2 achieves 0.1% PMD, in the TDL-C 100 ns channel at <1 dB higher SNR with AL-1, 2 and 4, 2 dB higher SNR with AL-8 and 3 dB higher SNR with AL-16. In the TDL-C 300 ns channel, PMD of Option 4 drops even more and the detection performance saturates to a final PMD value of 0.1-0.5%. It can be observed, that Option 4 tolerates frequency-selectivity better than Option 2 without the precoder cycling (Figure 13). Therefore, Option 4 has relatively good correlation properties, but on the other hand, it has four times more REs with the same AL. However, Option 4 cannot compete with Option 2 with precoder cycling (Figure 14). Because Option 4 is detected as a time-domain sequence, it cannot utilize precoder cycling and perform decisions from the combined smaller frequency parts.

It can be observed that Option 2 with AL-4, 8 and 16 (without precoder cycling), is comparable to the Option 4 with AL-1, 2 and 4. This is logical, since they have the same total amount of REs in a sequence. Between the above-mentioned cases, Option 2 has approximately 2 dB better performance in all of them.
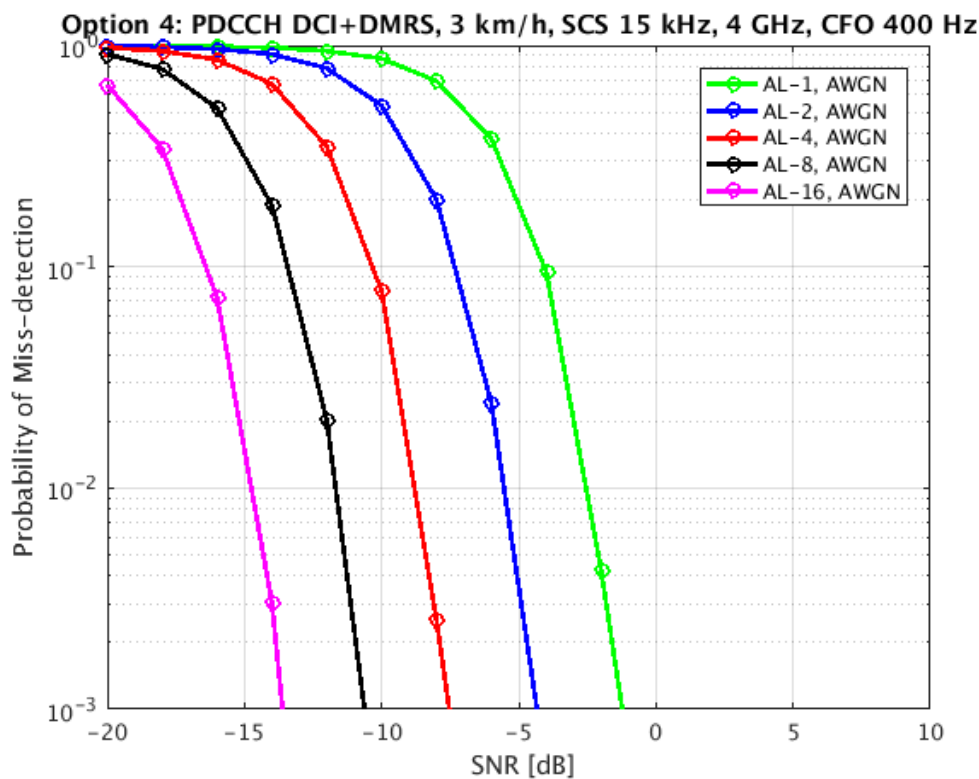

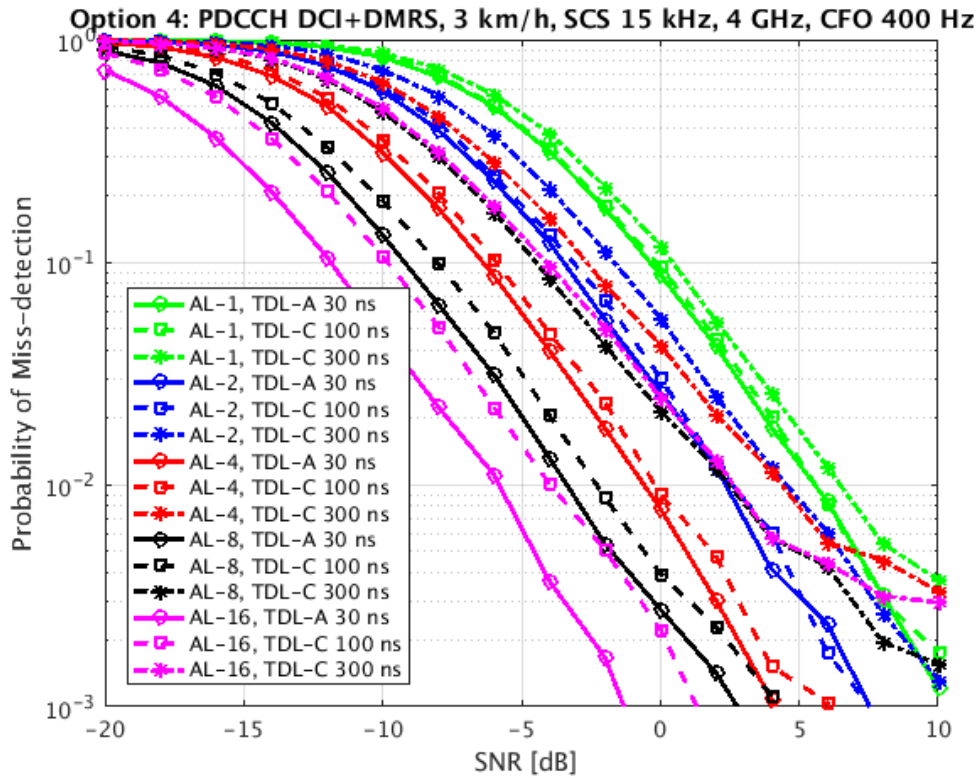Figure 16. Option 4 (PDCCH DCI+DMRS) in the AWGN channel.

Figure 17. Option 4 (DCI+DMRS) in TDL-A 30 ns, TDL-C 100 ns and TDL-C 300 ns channels.

The detection performance of Option 5 (regular PDCCH) in the AWGN channel is presented in Figure 18. It has PDCCH of sizes 6, 12, 24, 48 and 96 PRBs, which corresponds to aggregation levels 1, 2, 4, 8 and 16. As shown, doubling the number of the PRBs improves the SNR roughly 3 dB.

Option 5 (regular PDCCH) with al ALs, in TDL-A 30 ns, TDL-C 100 ns and TDL-C 300 ns channels is presented in Figure 19. As evidenced, the regular PDCCH is not so sensitive to the frequency-selective channel. In fact, with every AL, the detection performance is relatively same in TDL-C 100 ns and 300 ns channels, and 0.5 - 1 dB worse in the TDL-A 30 ns channel. In TDL-C 100 ns and 300 ns channels, the regular PDCCH with AL-16 has the best detection performance from the options, and in the TDL-A 30 ns channel it has the same performance as the PDCCH DMRS sequence with AL-16.
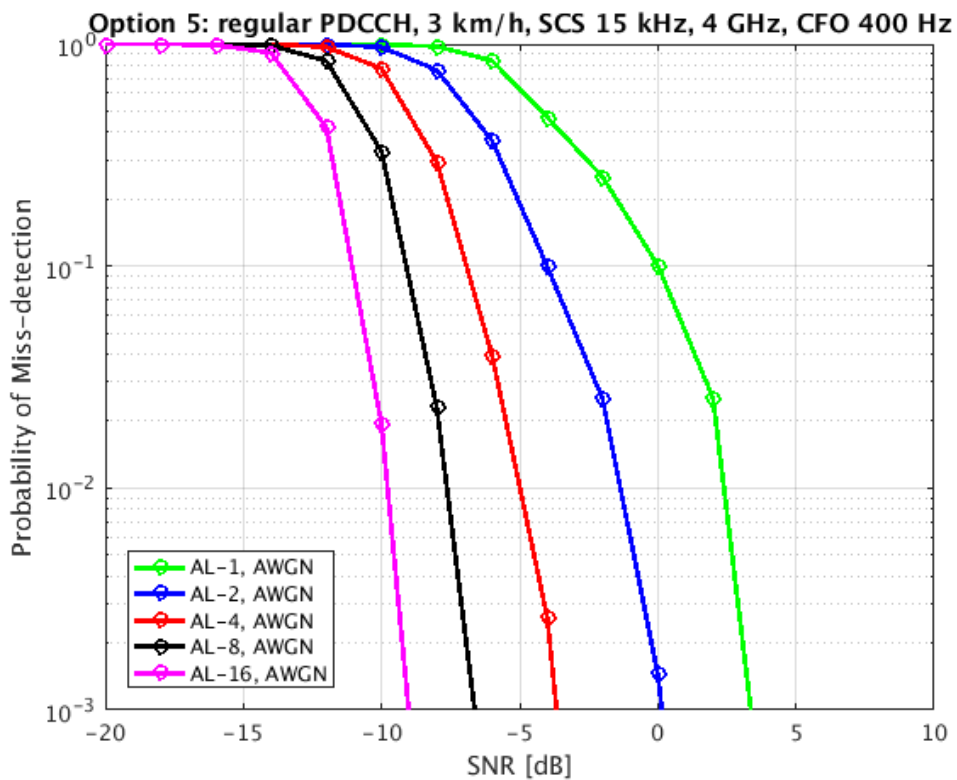
Figure 18. Option 5 (regular PDCCH) in the AWGN channel.
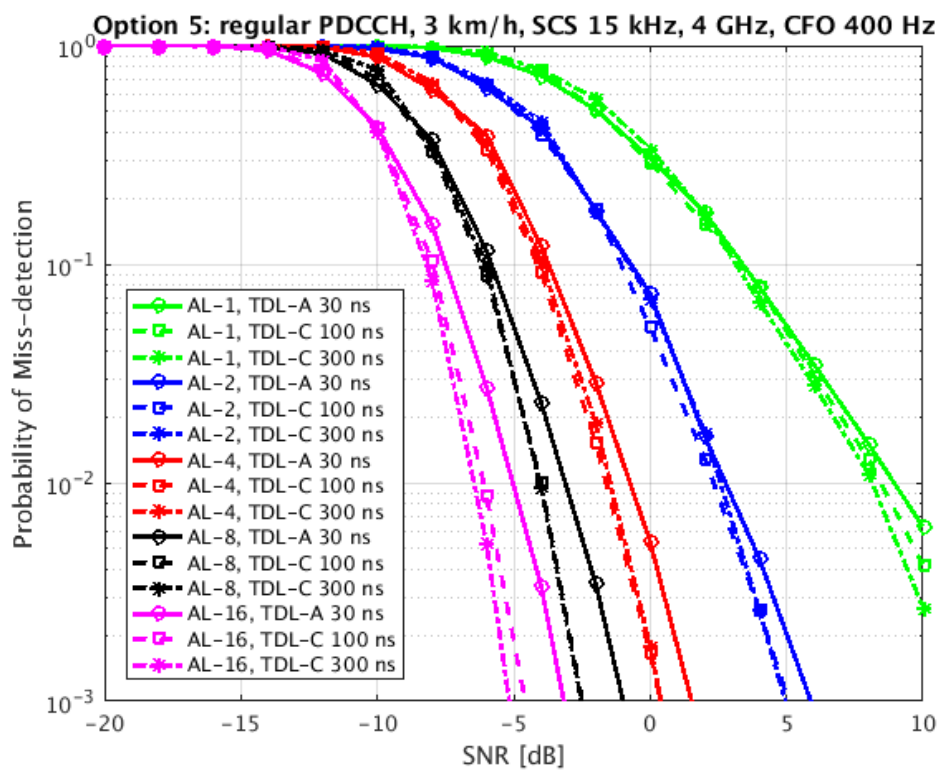

Figure 19. Option 5 (regular PDCCH) in TDL-A 30 ns, TDL-C 100 ns and TDL-C 300 ns channels.

As presented in Table 1 in Section 2.1, increasing the subcarrier spacing from 15 kHz to 30 kHz, halves the CP duration. Shortening the CP duration can problematic in a highly frequency-selective channel with a large Doppler spread. This is because CP should be longer than the channel's delay spread and the signal traverse time, otherwise the error detection deteriorates. However, doubling the SCS also doubles the bandwidth, which can cause problems in terms of frequency-selectivity.

Options 1-5 with 15 and 30 kHz SCSs in the TDL-C 100 ns channel are presented in Figure 20. As evident, the change in the subcarrier spacing has a minimalistic effect to Options 2 and 5 (the PDCCH DMRS and the regular PDCCH), but that is not the case with the other options. At 0.1% PMD, Option 1 (SSS) has 2 dB worse SNR with the 30 kHz SCS. However, Option 3 (CSI-RS/TRS) and Option 4 (the time-domain sequence PDCCH DCI+DMRS) have at least 5 dB worse performance with the 30 kHz SCS, at 1% PMD.

Options 1-5 with 15 and 30 kHz SCSs in a highly frequency-selective TDL-C 300 ns channel are presented in Figure 21. Therein, the change in the subcarrier spacing still has a minimalistic effect to Option 5, but now affects more Option 2. At 1% PMD, Option 2 has 1 dB worse performance with the 30 kHz SCS. With the 30 kHz SCS, Option 1 has 3 dB worse performance, Option 4 has 6 dB worse performance and Option 3 has over 10 dB worse performance. Time-selectivity from the weakened CP efficiency, combined with frequency-selectivity from the larger bandwidth, causes a significant detection performance deterioration in Options 1, 3 and 4.
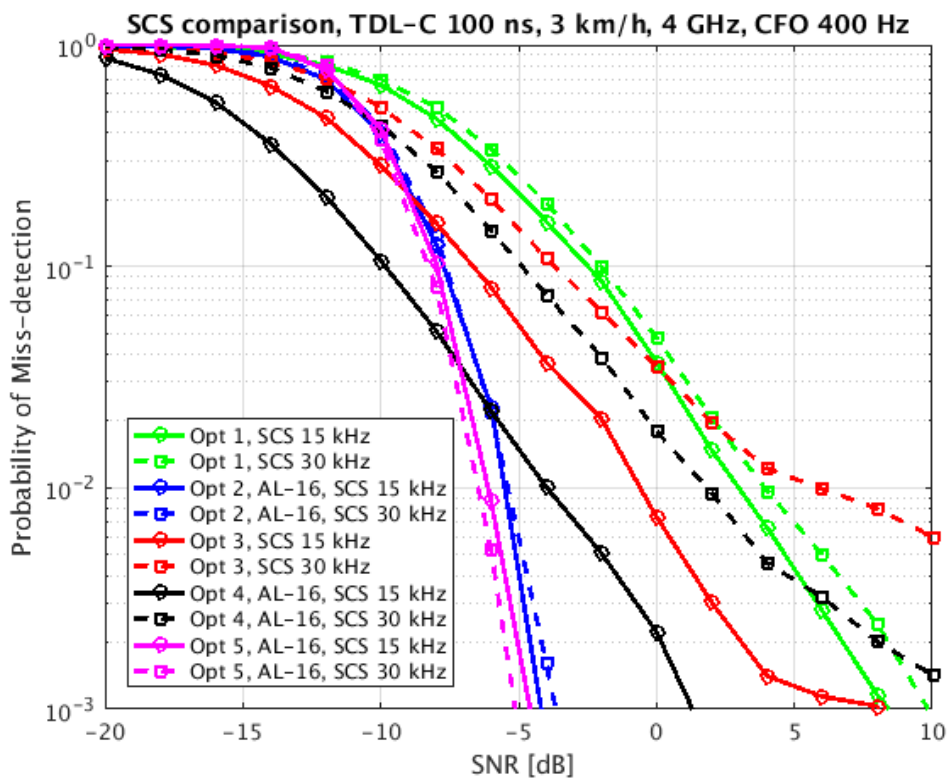

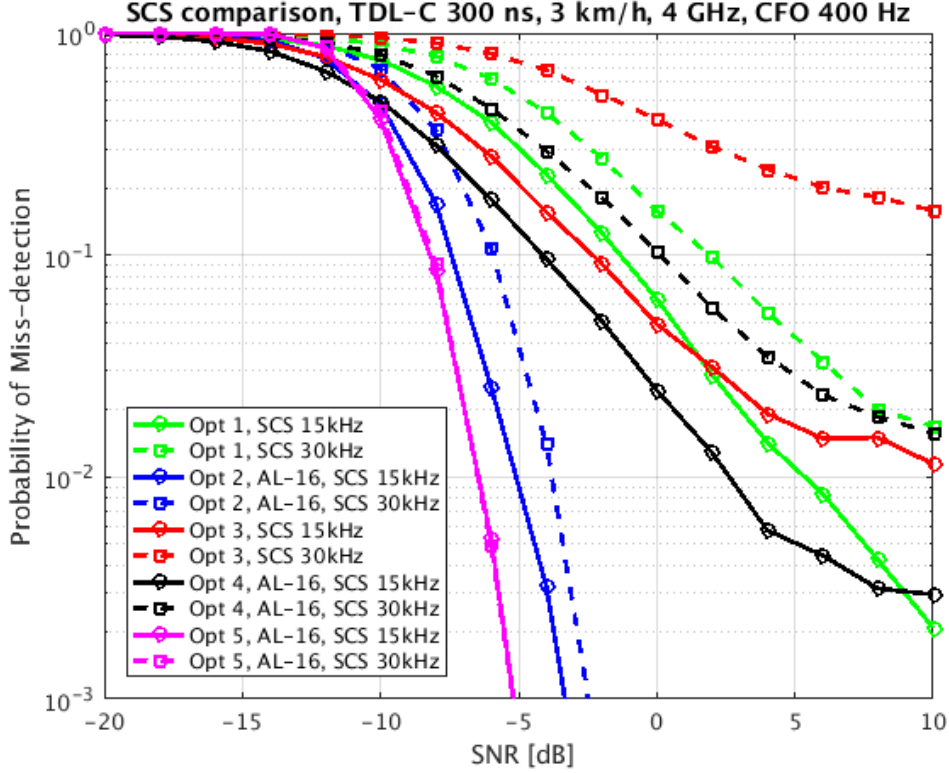Figure 20. A comparison of subcarrier spacings 15 & 30 kHz in the TDL-C 100 ns channel.

Figure 21. A comparison of subcarrier spacings 15 & 30 kHz in the TDL-C 300 ns channel.

5.2   Impact of the Time-Selectivity

As presented in (26) in Section 4.2, when the wavelength stays constant, the Doppler shift of the TDL channel increases in relation to velocity. The Doppler shift f_D is directly related to the Doppler spread B_D, because the Doppler spread is defined as the largest difference between Doppler shifts [36]. As presented in (25) in Section 4.2, the coherence time of the channel can be estimated as an inverse of the channel's Doppler spread. Therefore, increasing the UE speed increases the Doppler spread, and thus shortens the coherence time of the channel and causes time-selectivity.

Figures 22, 23 and 24 compare the impact of the UE speed to Options 1-5. In all these figures, solid lines present 3 km/h speed and dashed lines present 120 km/h speed. The impact of the UE speed in the TDL-C 100 ns channel with the 15 kHz SCS is presented in Figure 22. Figure 23 presents the impact of the UE speed in the TDL-C 300 ns channel with the 15 kHz SCS. Figure 24 presents the impact of the UE speed in TDL-C 300 ns channel with the 30 kHz SCS. As can be observed from Figures 22, 23 and 24, 120 km/h speed does not cause any significant deterioration to the detection performance of any of the options. Even with a highly frequency-selective TDL-C 300 ns channel and the 30 kHz SCS, all options have the same performance at both UE speeds. Only Option 3 has 0-2 dB deterioration of the detection performance with the 15 kHz SCS cases. For this reason, the impact of the UE speed up to 120 km/h can be neglected with Options 1, 2, 4 and 5. Option 3 is transmitted in two OFDM symbols and therefore it is more sensitive to time-selectivity. However, impact is relatively small, compared to the impact of the subcarrier spacing and channel in Section 5.1.
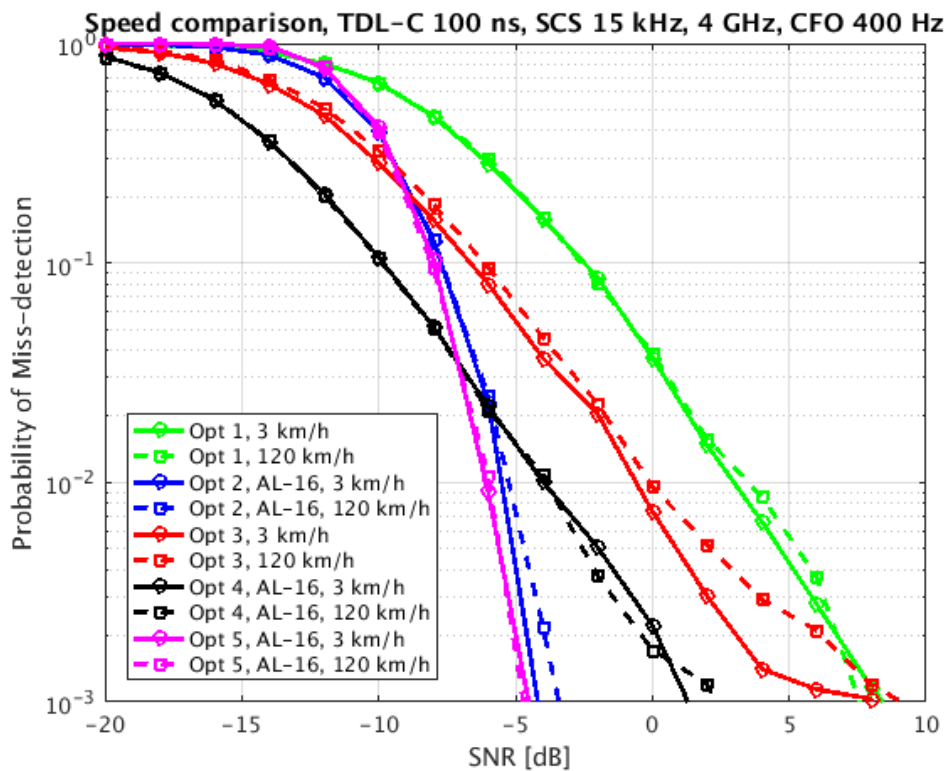
Figure 22. The impact of the UE speed in the TDL-C 100 ns channel with the 15 kHz SCS.
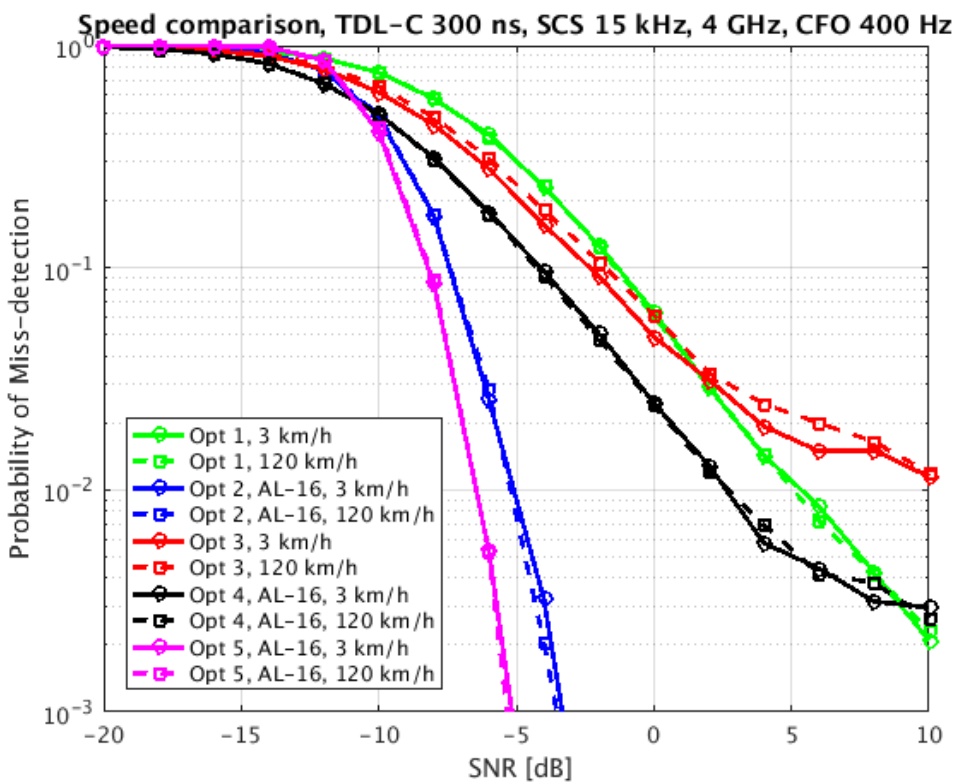

Figure 23. The impact of the UE speed in the TDL-C 300 ns channel, with the 15 kHz SCS.
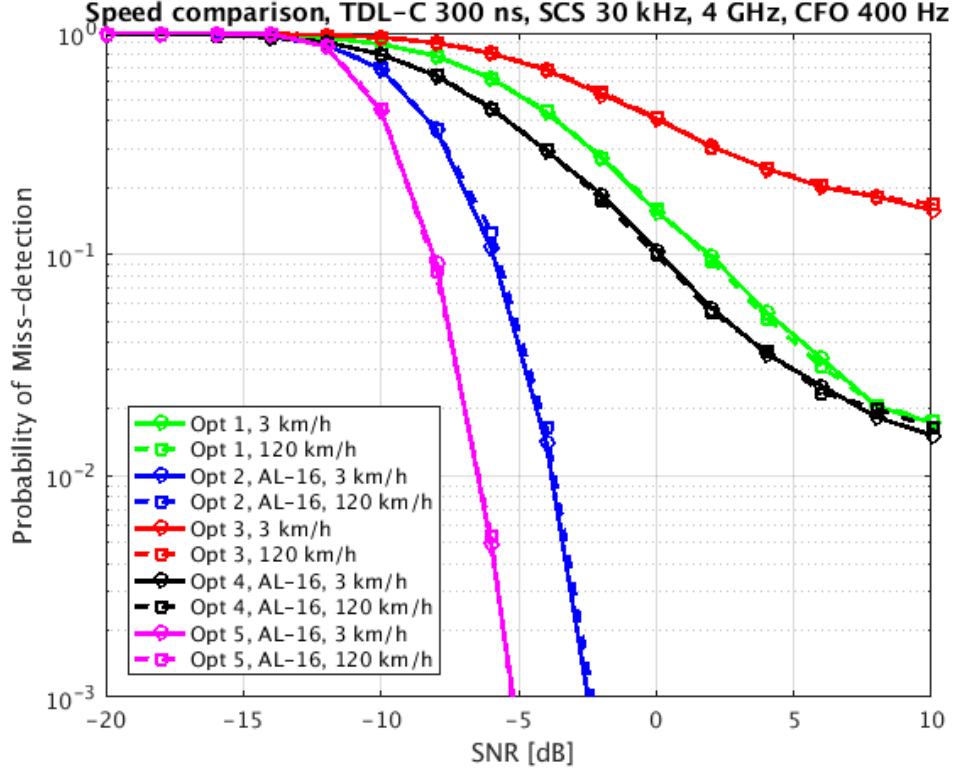
Figure 24. The impact of the UE speed in the TDL-C 300 ns channel, with the 30 kHz SCS.

5.3 Impact of the Implementation Impairments

Implementation impairments come from the non-idealities in the channels and systems. The carrier frequency offset is an implementation impairment that rotates the phase of the useful OFDM symbols [37]. Because of the phase offset between the transmitter and the receiver carriers, the receiver experiences a time-dependent phase rotation as a function of the frequency difference [38]. CFO causes inter-carrier interference (ICI) and affects orthogonality of the subcarriers [38]. Since the CFO can cause performance degradation, it is often estimated and compensated at the receiver [39].

In this work, the maximum carrier frequency offset in the simulations is 400 Hz. This value comes from the ±0.1 ppm (parts per million) frequency offset assumption, since 0.1 ppm × 4 GHz = 400 Hz. Figure 25 illustrates the impact of the 400 Hz carrier frequency offset to Options 1-5 in the TDL-C 100 ns channel and Figure 26 illustrates the impact in the TDL-C 300 ns channel. In both figures, the SCS is 15 kHz, the UE speed is 3 km/h, solid lines present the 0 Hz CFO and dashed lines present the 400 Hz CFO. As can be seen, the 400 Hz CFO does not cause any noticeable performance degradation to Options 1, 2, 4 and 5. Only Option 3 (CSI-RS/TRS) suffers from the 400 Hz offset. In the TDL-C 100 ns channel and with the 400 Hz CFO, Option 3 achieves 0.1% PMD at 3 dB larger SNR, compared to the 0 Hz CFO case. In the TDL-C 300 ns channel, Option 3 with the 400 Hz CFO achieves 1% PMD at 6 dB larger SNR, compared to the 0 Hz case. The rest of the options have approximately the same performance with and without the 400 Hz CFO. Therefore, Option 3 is sensitive to the CFO and the impact of it can be neglected with other options.
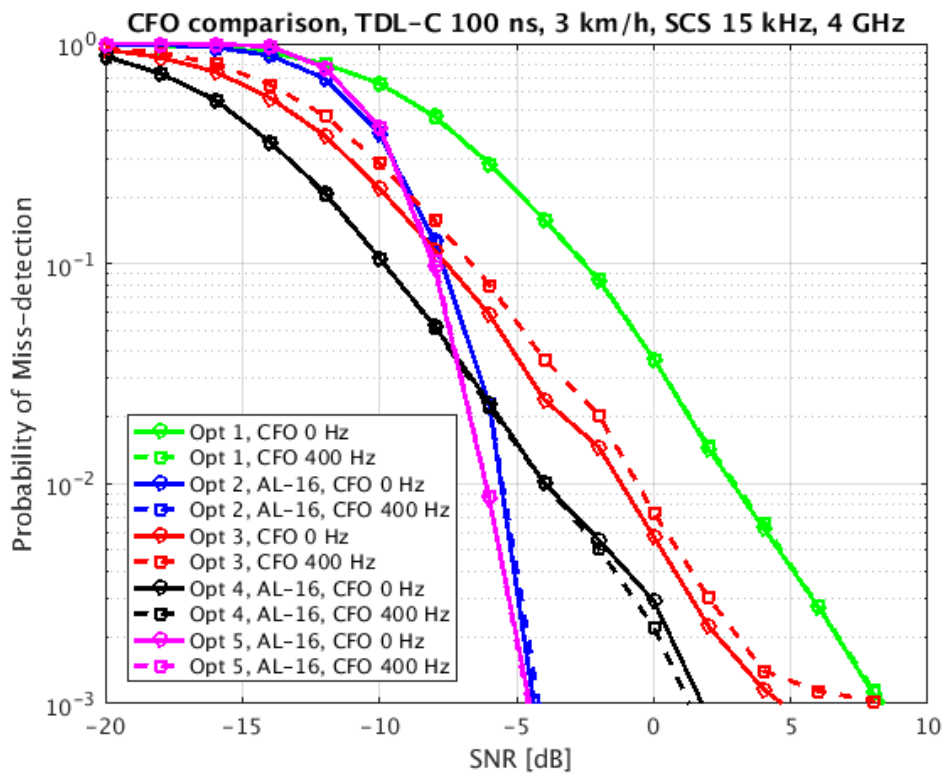
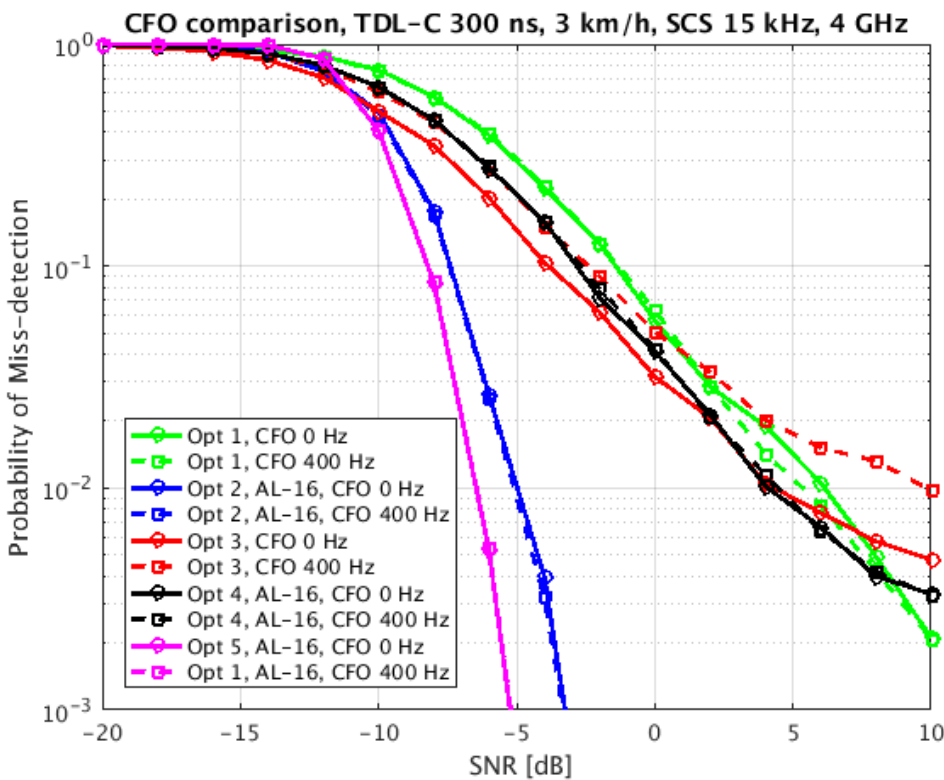Figure 25. The impact of the carrier frequency offset in the TDL-C 100 ns channel.

Figure 26. The impact of the frequency offset in the TDL-C 300 ns channel.

5.4   Impact of the Payload Size

As described in Section 3.3.3, PDCCH-based wake-up channel carries wake-up indication as a payload of its DCI. Depending on the format, payload size of the DCI can vary. In the earlier numerical results of this thesis, DCI payload of the PDCCH-based option has been 10 bits. In this section, impact of the DCI payload size is studied. Option 5 is simulated with DCI payload sizes of 10, 20 and 48 bits and in addition, a 24-bit CRC is attached to them.

   The impact of the DCI payload size to the detection performance of the PDCCH is presented in Figures 27-30. Figures 27 and 28 represents impact in the TDL-C 100 ns channel, with the 15 and 30 kHz SCS and Figures 29 and 30 in the TDL-C 300 ns channel with the 15 and 30 kHz SCS. In conclusion, the smaller payload size improves the detection performance in every case. For example, at 0.1% PMD, the difference between the SNR of the 10-bit and 48-bit payloads is 2.5 dB with AL-16, and 3.5 dB with AL-2. Therefore, the content of the DCI payload is an important design aspect, since the smaller payload provides better detection performance.

Figure 27. PDCCH payload comparison in the TDL-C 100 ns channel, with the 15 kHz SCS.

Figure 28. PDCCH payload comparison in the TDL-C 100 ns channel, with the 30 kHz SCS.
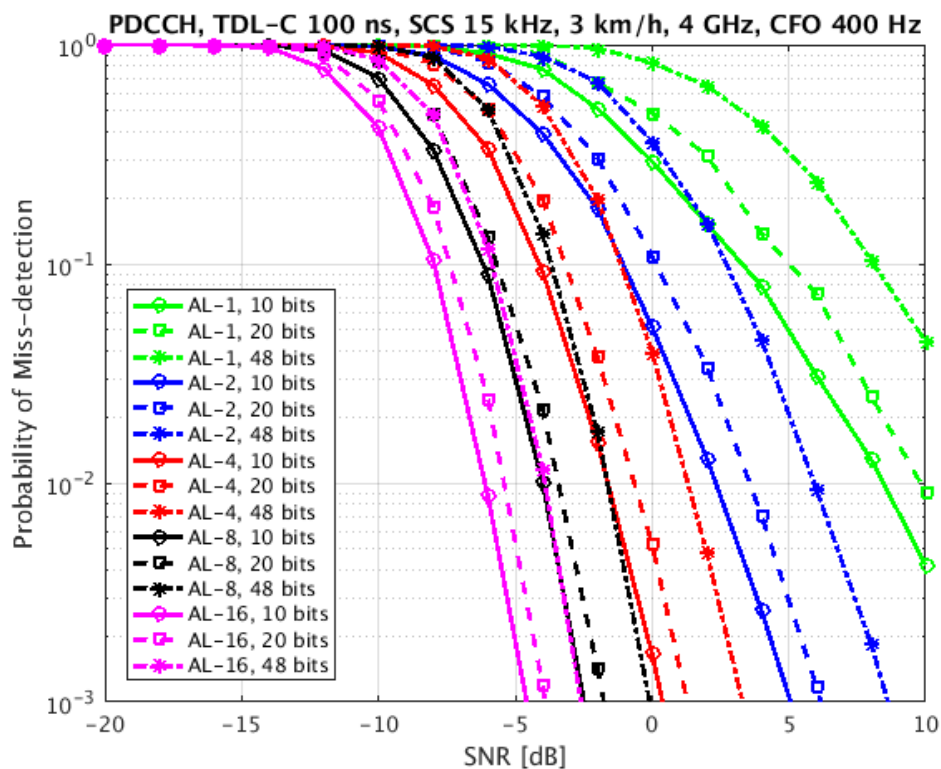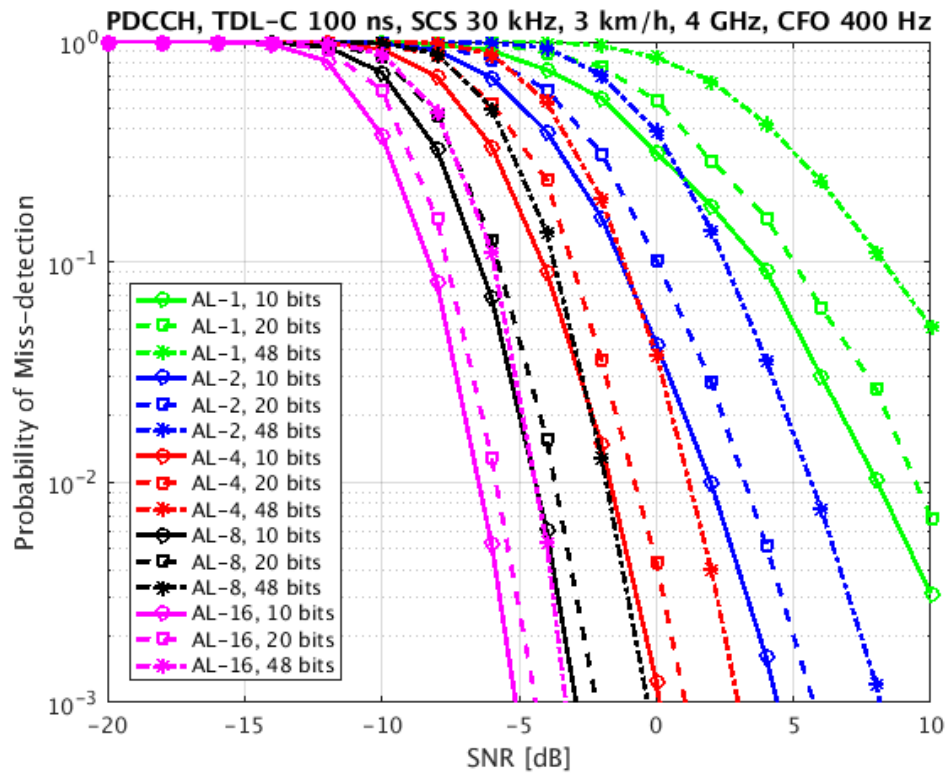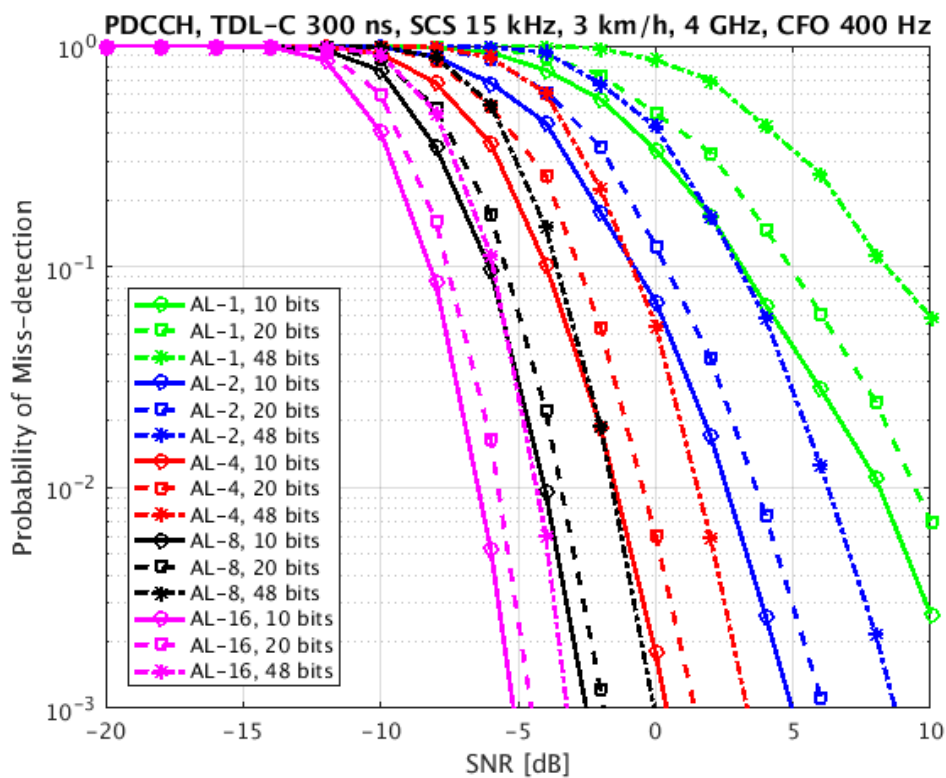

Figure 29. PDCCH payload comparison in the TDL-C 300 ns channel, with the 15 kHz SCS.
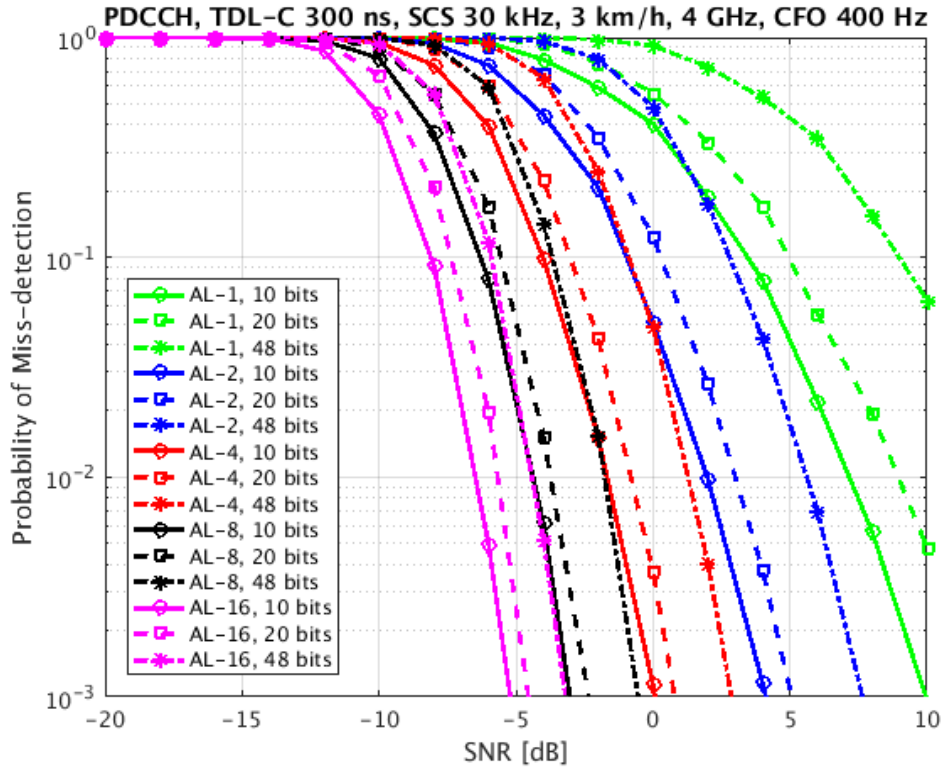
Figure 30. PDCCH payload comparison in the TDL-C 300 ns channel, with the 30 kHz SCS.

5.5 Summary of the Results

The summary of required SNR values to achieve <0.1% PMD for a set of WUS candidates in different cases is presented in Table 6. The WUS candidates are SSS, PDCCH DMRS with AL-16, CSI-RS/TRS, PDCCH DCI+DMRS with AL-16 and the regular PDCCH with AL-16. The cases are AWGN, TDL-A 30 ns and TDL-C 100 ns channels, with the 15 kHz SCS and 3 km/h UE speed, as well as the TDL-C 300 ns channel with the 30 kHz SCS and 120 km/h UE speed. In Table 6, the AWGN case represents the ideal case, while TDL-C 300 ns with the 30 kHz SCS and 120 km/h UE speed represents the worst-case scenario. In the AWGN channel, all candidates from Table 4 achieve the target 0.1% PMD at ≤-4 dB SNR. With the TDL-A 30 ns channel, 3 km/h UE speed and 15 kHz SCS, the SNR of Options 2 and 5 is -3.5 dB, the SNR of Option 4 is -2 dB and the other options are over 10 dB away from the target SNR. In the TDL-C 100 ns channel, 3 km/h UE speed and 15 kHz SCS, the SNR of Option 2 is -4.5 dB and the SNR of Option 5 is -5 dB, and the other options are over 8 dB away from the target SNR. In the TDL-C 300 ns channel, 120 km/h UE speed and 30 kHz SCS, the SNR of Option 2 is -2.5 dB and the SNR of Option 5 is -5 dB, and the other options do not meet the target before 10 dB, but instead saturate to a certain PMD point.

Two important observations can be made from Table 6. Firstly, Options 1, 3 and 4 are sensitive to frequency-selectivity, but Options 2 and 5 endure them well. Secondly, Option 5 with AL-16 has a better or equal detection performance than Option 2 with AL-16, in every simulation case.

Table 6. The required SNR value to achieve ≤0.1% probability of miss-detection.

WUS candidate	AWGN SCS 15 kHz 3 km/h	TDL-A 30 ns SCS 15 kHz 3 km/h	TDL-C 100 ns SCS 15 kHz 3 km/h	TDL-C 300 ns SCS 30 kHz 120 km/h
Option 1: SSS	-4.5 dB	8 dB	8 dB	-
Option 2: PDCCH DMRS AL-16	-9.5 dB	-3.5 dB	-4.5 dB	-2.5 dB
Option 3: CSI-RS/TRS	-8 dB	4 dB	8 dB	-
Option 4: PDCCH DCI+DMRS AL-16	-14 dB	-2 dB	2 dB	-
Option 5: PDCCH regular AL-16	-9 dB	-3.5 dB	-5 dB	-5 dB

6 DISCUSSION

As discussed in Section 3.3, with the WUS functionality, the UE can achieve power saving. The relative amount of power saving depends on the circumstances and the DRX configuration. With a long DRX cycle, the relative power saving is smaller, because of the fewer unneeded PDCCH monitoring occasions that can be skipped with the WUS. The relative power saving is larger with a short DRX cycle, because it has more frequent PDCCH monitoring occasions. Since the WUS functionality can offer power saving, it would be a reasonable added feature to the NR. In this work, five different signal/channel options for the WUS were compared based on detection performance simulations.

As can be observed from the simulation results, in the AWGN channel, the total number of REs dominate the detection performance of the WUS options. PDCCH DMRS, PDCCH DCI+DMRS and the regular PDCCH have one OFDM symbol in time, and they can be configured in five different lengths. In AWGN and not very frequency selective TDL-A 30 ns channels, doubling the number of REs results to approximately 3 dB gain in all these cases. However, doubling the number of REs also doubles the bandwidth. In a somewhat frequency-selective channel, the performance of the CSI-RS and PDCCH DCI+DMRS drops slightly. In a very frequency-selective TDL-C 300 ns channel, the large bandwidth becomes a real problem. CSI-RS/TRS as well as PDCCH DCI+DMRS and PDCCH DMRS sequences with $\geq$12 PRBs saturate to a point, where increasing the SNR does not improve the performance. However, during this study it is observed that the precoder cycling and making detection in parts, improves the detection performance of the PDCCH DMRS sequence in all fading channels. Making the decisions in smaller frequency parts and combining results ensures that the decisions are made within the channel's coherence bandwidth.

Since the detection of the PDCCH DCI+DMRS sequence is done in the time domain, the decisions cannot be made in smaller frequency parts, like with the PDCCH DMRS sequence. Even though PDCCH DCI+DMRS with AL-16 is the longest sequence from the sequence-based options, it cannot compete with the regular PDCCH or the PDCCH DMRS sequence. In the AWGN channel, PDCCH DCI+DMRS with ALs 2, 4, 8 and 16 meet the target 0.1% PMD at $\leq$-4 dB SNR, but it cannot meet the target in any of the fading channels. CSI-RS/TRS based sequence tolerates frequency-selective channels very poorly, and it meets the target 0.1% PMD at $\leq$-4 dB SNR only in the AWGN channel. The SSS based sequence tolerates frequency-selective channels better, but it too meets the target 0.1% PMD at $\leq$-4 dB SNR only in the AWGN channel.

Some of the numerical results presented in this thesis and earlier results simulated during this work have been used for example in Nokia's 3GPP contributions R1-1903135 [40] and R1-1905384 [41]. To validate the presented results, there are some simulation benchmarks from participating companies in their 3GPP contributions. Generally, the results presented in this thesis seem to be well-aligned with their counterparts [5]. However, the comparison is complicated by differences in the simulation configurations, such as channel models, antenna configurations, payload sizes and time/frequency allocations.

The performance of the WUS is always limited by the detection performance of the actual PDCCH transmission. If the UE cannot receive and decode PDCCH at all, there is no point to wake up to receive it. Therefore, the detection performance of the WUS should be at least as good as the detection performance of the PDCCH transmission, but it does not have to be considerably better. Because of this, the requirements can be relaxed in that respect.

The detection performance is a trade-off between a false alarm and detection probability. If the probability of false alarm is larger, the probability of miss-detection is smaller. However, if

the UE often wakes up needlessly, unnecessary power consumption increases. So, the probability of false alarm is a trade-off between detection performance and power consumption. Therefore, the probability of false alarm should be manageable, so that the miss-detection probability is good enough, but power consumption does not increase needlessly.

The strongest design options for power saving signal/WUS are the regular PDCCH with AL-16 and the PDCCH DMRS sequence with AL-16. The PDCCH can take the advantage of coding and channel estimation. Yet, they both can utilize precoder cycling as a diversity scheme, and they meet the target miss-detection probability even in a very frequency-selective channel. However, the AL-16 regular PDCCH outperforms the AL-16 PDCCH DMRS in all simulation cases, except in the TDL-A 30 ns channel, where they have a similar performance. For that reason, the regular PDCCH is the most robust option for power saving signal/channel, in terms of the detection performance.

If the power saving signal/channel design would be based-on PDCCH, the actual wake-up indication can be smaller (for example 1-2 bits) than the PDCCH DCI payload [5]. It could be beneficial that the overall size of the PDCCH-based WUS is the same as the size of the other PDCCHs configured to that UE. This way, impact to the NR standardization and implementation processes would be more feasible. It would also mean that in addition to wake-up triggering, PDCCH-based power saving channel could carry additional information in its payload and/or trigger other power saving mechanisms. Therefore, actual format, size and content of the DCI would need to be determined. DCI format could be for example the same size as some existing DCI format, but designed for power saving/wake-up triggering purposes. However, as observed in Section 5.4, payload size is a tradeoff between size and detection performance, so the more compact the payload is, the better.

In this work, only one CORESET size and non-interleaved frequency/time allocation is studied. If the WUS design would be based on the PDCCH, the frequency/time allocation can also be interleaved, as described in Section 2.2.3. The interleaved allocation could potentially provide more frequency diversity and with it, better performance. In the future, it would be also beneficial to study the beam-level behavior and the impact of beamforming to detection performance. It should also be considered, whether the WUS is scalable or not. For example, in the cell edge, the WUS could be configured to use AL-16, and closer to the center of the cell the WUS could use smaller aggregation levels, like AL-8 or AL-4.

7 SUMMARY

The objective of this thesis was to study and evaluate physical layer signals and channels to achieve UE power saving in 5G NR. First, an overview of the general properties of the NR physical layer and downlink signals/channels was provided. Then, the operation principles of RRC states and power consumption in the CONNECTED state were described.

Examples of existing power saving techniques in the time and the frequency domain were provided, and a new concept of the power saving signal/channel was introduced. One use-case for the power saving signal is to trigger the UE for network access from the power saving mode. In this thesis, this operation is referred to as the wake-up operation, and the power saving signal/channel in this context is called the wake-up signal (WUS). The power saving potential of the WUS was described, as well as the design options and details. The exact amount of the UE power saving heavily depends on the usage scenario. Especially, the length of the DRX cycle and the on-period impact heavily to the relative power saving gain. Depending on the reference case, the WUS could provide 8% - 50% relative power saving gain to the UE.

WUS design candidates are based on the existing NR Release 15 physical signals/channels. The analysis is based on the 3GPP NR compliant link-level simulations. Numerical results were presented in terms of the probability of miss-detection as a function of the SNR. In this thesis, five different physical layer signal/channel options for the WUS were studied. The options were frequency-domain sequences SSS, PDCCH DMRS and CSI-RS/TRS, the time-domain sequence PDCCH DCI+DMRS and the regular PDCCH.

Numerical detection performance results study the impact of the frequency- and time-selectivity, as well as implementation impairments. One of the main observations regarding frequency-selectivity, is that the total number of REs dominates the detection performance in AWGN and non-frequency selective channels. However, in somewhat and/or highly frequency-selective channels, the large bandwidth included with a large number of REs may become a problem. A large bandwidth can exceed the channel's coherence bandwidth, which causes distortion and corrupts the signal. However, the impact of the frequency-selectivity can be decreased with the use of diversity techniques like precoder cycling. During this work, it was also observed that making decisions in smaller parts, within the channel's coherence bandwidth, can be used to improve the detection performance.

Larger subcarrier spacing can cause problems in terms of both the frequency- and the time-selectivity. Doubling the SCS doubles the bandwidth, which in many cases causes the signal bandwidth to exceed the coherence bandwidth even more. Moreover, doubling the SCS can also cause time-selectivity, because of the shorter CP duration. In turn, larger velocity of a transceiver increases the Doppler spread of the radio channel and thus causes time-selectivity by shortening the coherence time. Carrier frequency offset is an implementation impairment, that can cause performance degradation to the system. Based on the numerical results, CSI-RS/TRS is the only option that is prone to time-selectivity and carrier frequency offset. The impact of the UE speed up to 120 km/h and CFO up to 400 Hz can be neglected with all the other options.

In conclusion, from the sequence-based options, PDCCH DMRS is the only one that can compete with the PDCCH based option. The rest of the sequence-based options either saturate to a certain miss-detection probability or do not meet the target performance. However, PDCCH outperforms the PDCCH DMRS sequence in most of the cases. Based on the numerical results, the PDCCH based WUS is the most robust option in terms of the detection performance.

8   REFERENCES

[1]   Dahlman E., Parkvall S., Sköld J (2018) 5G NR: The Next Generation Wireless Access Technology. Academic Press, 466 p.

[2]   ITU-R (2015) IMT Vision – Framework and overall objectives of the future development of IMT for 2020 and beyond. ITU-R Recommendation M.2083-0.

[3]   Ji H., Park S., Yeo J., Kim Y., Lee J. & Shim B. (2018) Ultra-Reliable and Low-Latency Communications in 5G Downlink: Physical Layer Aspects. IEEE Wireless Communications, Volume 25, Issue 3, p. 124-130.

[4]   Lauridsen M., Noel L., Sorensen T. & Mogensen P. (2014) An Empirical LTE Smartphone Power Model with a View to Energy Efficiency Evolution. Intel Technology Journal, Volume 18, Issue 1, p. 172-193.

[5]   3GPP. (2019) Study on UE Power Saving. Technical Report 38.840, Version 1.0.0, Release 16.

[6]   3GPP. (2017) Services provided by the physical layer. Technical Specification 38.201, Version 15.0.0, Release 15.

[7]   Sesia S., Toufik I. & Baker M. (2011) LTE - The UMTS Long Term Evolution: From Theory to Practice, Second Edition. A John Wiley & Sons, Ltd., Publication, United Kingdom.

[8]   Lien S., Shieh S., Huang Y., Su B., Hsu Y. & Wei H. (2017) 5G New Radio: Waveform, Frame Structure, Multiple Access and Initial Access. IEEE Communications Magazine, Volume 55, Issue 6, p. 64-71.

[9]   Vihriälä J., Zaidi A., Venkatasubramanian V., He N., Tiirola E., Medbo J., Lähetkangas E., Werner K., Pajukoski K., Cedergren A. & Baldemair R. (2016) Numerology and Frame Structure for 5G Radio Access. In: IEEE 27th Annual International Symposium on Personal, Indoor, and Mobile Radio Communications (PIMRC). Workshop IRACON2016.

[10]   3GPP. (2019) Physical channels and modulation. Technical Specification 38.211, Version 15.5.0, Release 15.

[11]   Sharetechnote (read 9.4.2019) 5G/NR – Frame Structure. URL: http://www.sharetechnote.com/html/5G/5G_FrameStructure.html

[12]   Zaidi A., Baldemair R., Andersson M., Faxér S., Molés-Cases V. & Wang Z. (2017) 5G New Radio: Designing for the future, Ericsson technology Review. Ericsson AB, Sweden, Stockholm.

[13] Lin X., Li J., Baldemair R., Cheng T., Parkvall S., Larsson D., Koorapaty H., Frenne M., Falahati S., Grövlen A. & Werner K (2018) 5G New Radio: Unveiling the Essentials of the Next Generation Wireless Access Technology. Ericsson

[14] 3GPP. (2019) Physical layer procedures for control. Technical Specification 38.213, Version 15.5.0, Release 15.

[15] Campos J. (2017) Understanding the 5G NR Physical Layer. Keysight Technologies.

[16] Lin Z., Li J., Zheng Y., Irukulupati N., Wang H. & Sahlin H. (2018) SS/PBCH Block Design in 5G New Radio (NR). In: 2018 IEEE Globecom Workshops (GC Wkshps), December 9-13, Abu Dhabi, United Arab Emirates.

[17] Hamidi-Sepehr F., Kwak Y., Chatterjee D. (2018) 5G NR PDCCH: Design and Performance. In: IEEE 5G World Forum (5GWF), July 9-11, Silicon Valley, CA, USA, Vol. 1, p. 250-255, Santa Clara.

[18] Miao H. & Faerber M. (2017) Physical Downlink Control Channel for 5G New Radio. In: 2017 European Conference on Networks and Communications (EuCNC), 12-15 June, Oulu, Finland.

[19] R1-1705224 (2017) Evaluation of transmission/diversity schemes for DL control channel. 3GPP TSG RAN WG1 Meeting #88, Spokane, WA, USA.

[20] 3GPP. (2017) Study on New Radio Access Technology, Physical Layer Aspects. Technical Report 38.802, Version 14.2.0, Release 14.

[21] 3GPP. (2019) Physical layer procedures for data. Technical Specification 38.214, Version 15.5.0, Release 15.

[22] Ryoo S., Jung J. & Ahn R. (2018) Energy Efficiency Enhancement with RRC Connection Control for 5G New RAT. In: 2018 IEEE Wireless Communications and Networking Conference (WCNC), April 15-18, Barcelona, Spain.

[23] 3GPP. (2017) Study on Scenarios and Requirements for Next Generation Access Technologies. Technical Report 38.913, Version 14.3.0, Release 15.

[24] Wang H. C., Tseng C. C., Chen G. Y., Kuo F. C. & Ting K. C. (2013) Power saving by LTE DRX mechanism using mixture of short and long cycles. In: 2013 IEEE International Conference of IEEE Region 10 (TENCON 2013), October 22-25, Xi'an, China.

[25] Liang J., Hsieh P., Chen J. and Tseng Y. (2013) Energy-Efficient DRX Scheduling for Multicast Transmissions in 3GPP LTE-Advanced Wireless Networks. In: 2013 IEEE Wireless Communications and Networking Conference (WSNS): MAC, April 7-10, Shanghai, China.

[26] 3GPP. (2019) Medium Access Control (MAC) protocol specification. Technical Specification 38.321, Version 15.5.0, Release 15.

[27] Jeon J. (2018) NR Wide Bandwidth Operations. IEEE Communications Magazine, Volume 56, Issue 3, p. 42-46.

[28] IEEE Innovation at work. (read. 10.4.2019) Make Batteries Last Longer: IEEE 802.11 Wake-Up Radio. URL: https://innovationatwork.ieee.org/make-batteries-last-longer-ieee-802-11-wake-up-radio/

[29] Prete M., Masotti D., Costanzo A, Magno M & Benini L (2016) A Dual-Band Wake-Up Radio for Ultra-low Power Wireless Sensor Networks. In: IEEE 2016 IEEE Topical Conference on Wireless Sensors and Sensor Networks (WiSNet), January 24-27, Austin, TX, USA.

[30] R1-1903133 (2019) Comparison of DRX with WUS and GTS schemes. 3GPP TSG RAN WG1 Meeting #96, Athens, Greece.

[31] MathWorks. (read 7.2.2019) MATLAB. URL: https://www.mathworks.com/help/matlab

[32] Sklar B. (1997) Rayleigh Fading Channels in Mobile Digital Communication Systems Part 1: Characterization. In: IEEE Communication Magazine, Vol 35, Issue 7, p. 90-100.

[33] Proakis J. (2001) Digital Communications, Fourth Edition. McGraw-Hill, New York, USA.

[34] 3GPP. (2018) Study on channel model for frequencies from 0.5 to 100 GHz. Technical Report 38.901, Version 15.0.0, Release 15.

[35] ITU-R. (2017) Guidelines for evaluation of radio interface technologies for IMT-2020.

[36] Tse D. & Viswanath P. (2005) Fundamentals of Wireless Communication. Cambridge University Press, Cambridge, UK.

[37] Pollet T., Van Bladel M. & Moeneclaey M. (1995) BER sensitivity of OFDM systems to carrier frequency offset and Wiener phase noise. In: IEEE Transactions on Communications, Volume 43, Issue 2/3/4, p. 191-193.

[38] Fouladifard S. & Shafiee H. (2003) Frequency Offset Estimation in OFDM Systems in Presence of IQ Imbalance. In: IEEE International Conference on Communications, 2003 (ICC '03), May 11-15, Anchorage, AK, USA.

[39] Singh P. & Vasudevan K. (2017) Preamble-based Synchronization for OFDM/OQAM Systems in AWGN Channel. In: 2017 4th International Conference on Signal Processing and Integrated Networks (SPIN), February 2-3, Noida, India.

[40] R1-1903135 (2019) On potential power saving triggering signals. 3GPP TSG RAN WG1 Ad-Hoc Meeting #96, Athens, Greece.

[41] R1-1905384 (2019) PDCCH-based power saving signal/channel. 3GPP TSG RAN WG1 #96bis, Xi'an, China.